Title
MECHANICAL BEHAVIOR OF SINGLE-CRYSTAL AND POLY-CRYSTALLINE CESIUM BROMIDE

Authors
Johnson, Lawrence D.
Pask, Joseph A.

Publication Date
1962-09-01

UCRL-10468

University of California

Ernest O. Lawrence Radiation Laboratory

MECHANICAL BEHAVIOR OF SINGLE AND POLYCRYSTALLINE CESIUM BROMIDE

Berkeley, California

DISCLAIMER

UCRL-10468
UC-25 Metals, Ceramics,
and Materials
TID-4500 (18th Edition)

Research and Development

UNIVERSITY OF CALIFORNIA

Lawrence Radiation Laboratory
Berkeley, California

Contract No. W-7405-eng-48

MECHANICAL BEHAVIOR OF SINGLE AND POLYCRYSTALLINE CESIUM BROMIDE

Lawrence D. Johnson
(Thesis)

September 12, 1962

Printed in USA. Price $2.00. Available from the
Office of Technical Services
U. S. Department of Commerce
Washington 25, D.C.

THE MECHANICAL BEHAVIOR OF SINGLE AND POLYCRYSTALLINE CESIUM BROMIDE

Contents

MECHANICAL BEHAVIOR OF SINGLE AND POLYCRYSTALLINE CESIUM BROMIDE

Lawrence D. Johnson

Lawrence Radiation Laboratory
University of California
Berkeley, California

September 12, 1962

ABSTRACT

Plastic-deformation experiments were conducted on cesium bromide, a material that lacks cleavage planes, to study the effect of the absence of cleavage on the mechanical behavior. Observations were made and theories were proposed concerning the mechanisms of plastic deformation and fracture in cesium bromide.

Single-crystal cesium bromide was found to be soft and ductile if it was favorably oriented relative to the loading axis to activate the $\{110\}\ \langle 100 \rangle$ slip systems. Kink bands were formed by directing a compression load normal to the $\{100\}$ system of planes. Cross-slip was found to occur during deformation at all test temperatures. Tensile and bending loads directed normal to $\{100\}$ and $\{110\}$ planes caused fracture on $\{110\}$ planes, while compressive loads normal to $\{100\}$ planes forced fracture on $\{112\}$ planes rather than $\{110\}$ planes.

The ductility of polycrystalline cesium bromide was found to decrease for samples with smaller grain sizes. The absence of a sufficient number of slip systems in the specimens may have been responsible for this plastic behavior. The mechanism of fracture was intergranular in polycrystalline cesium bromide.

I. INTRODUCTION

A considerable number of investigations concerning the mechanical behavior of rock salt structure (interpenetrating face-centered cubic) ionic single crystals have been made, particularly because of the ease in preparing suitable specimens and the relative simplicity of plastic deformation by the six $\{110\}$ $\langle 110 \rangle$ glide systems. A better understanding of the mechanical behavior of such crystals is still desired, however, because of the limitations of plastic deformation caused by the $\{100\}$ cleavage fracture[1-4] in many of these crystals. It was consequently felt that an investigation of the mechanical behavior of an ionic crystal that does not possess cleavage planes and a comparison of the mechanical behavior of such a crystal with those which do have cleavage would be of interest. Such an ionic crystal, with no cleavage at room temperature, is cesium bromide (interpenetrating simple cubic structure). There have been a number of investigations concerning the mechanical properties of cesium bromide in the past, but the effect of the absence of cleavage fracture on its mechanical behavior had not been considered.

The investigation reported herein is concerned with the mechanical behavior of single crystal and polycrystalline cesium bromide, and the effect of the lack of cleavage on the mechanical behavior of the material. This report covers a general review of the past experimental work concerning single-crystal cesium bromide and some polycrystalline agregates, and then seeks to explain the mechanisms of plastic deformation and fracture with the absence of cleavage in both single-crystal and polycrystal material.

II. REVIEW OF LITERATURE

A. Mechanism of Slip

Slip in ionic single crystals will take place most favorably on planes of high atom density and in directions where the movement of the ions will not create electrostatic repulsive forces. That is, the atoms will not move in directions that will cause cations to be in nearest-neighbor positions. These considerations indicate that thallium halide and cesium bromide type ionic crystals should deform plastically by slip on the $\{110\}$ $\langle 100 \rangle$ slip systems. This has been confirmed by several experimental investigations.[5-8] Flow on other slip systems has not been observed.

B. Kink-Band Formation

If cesium chloride type single crystals are oriented so that deformation loads are applied normal to $\{100\}$ planes, then the shear stress acting on the $\{100\}$ $\langle 100 \rangle$ slip systems is zero. This result is calculated[9] by

$$\sigma_R = \sigma_A \cos\theta \cos\lambda, \qquad (1)$$

where

σ_R is the resolved shear stress,
σ_A is the applied stress,
θ is the angle between the normal to the plane and the load axis, and
λ is the angle between the slip direction and the load axis.

The resolved stress is the stress that acts on a certain plane in a certain direction for a particular orientation of the applied load. Zemtsov et al.[10] have shown that for compression loads applied normal to $\{100\}$ planes on thallium halide type crystals, deformation was brought about entirely by rotation of the lattice forming fault zones (kink bands) within the lattice. Kink bands result from a process of organized slip of edge dislocations on many parallel planes. Kink planes, which are usually

seen with kink bands, are lines of discontinuity where the crystal abruptly changes its orientation. These bands are constructed of many edge dislocations of the same sign. Zemtsov et al. reported that the formation of these kink bands was accompanied by a loud "crack" and the formation of tiny fissures.

Orowan[11] found a similar phenomenon in cadmium crystals that were loaded in compression and oriented so that the (001) glide plane did not operate. After a sufficiently high load was applied, the crystal suddenly collapsed by forming peculiar kink planes having sharp ridges and regular curvatures. It was concluded that the non-crystallographic orientation of the kinks, the regular curvatures, and certain other features ruled out the possibility of glide or twinning, and that, rather, the phenomenon represented kink bands.

Studies of TlI-TlBr and CsI by Kolontsova et al.[12] and Kolontsova and Telegina[13, 14] indicated that the area within the kink planes separated into further wedge-shaped blocks turned relative to one another. These wedge-shaped areas seemed to be bounded by sharp lines ("sliding lines") in TlI-TlBr cyrstals. Kolontsova et al.[12] suggested from their results that the kinks could have been caused by twinning on {11h} type planes where h seemed to be about 8, and that the sliding lines between the wedge-shaped areas were brought about by kinking, as suggested by Orowan.[11] (A twin plane is a plane across which there is found a mirror reflection of the lattice.)

Klassen-Neklyudova and Urusovskaya[15, 16] also observed kinks in TlI-TlBr and CsBr of non-crystallographic boundaries and wedge-shaped regions within the kinks. The appearance of the kink bands was accompanied by a cracking sound and seemed to be correlated with the formation of large numbers of cracks within the kinked region. The kink bands were formed only when glide was impossible and when a nonuniform stress state existed in the specimen. A uniform tensile stress normal to the {100} family of planes failed to produce kinking. Klassen-Neklyudova and Urusovskaya further found that rupture occured in the

majority of cases along the {110} planes, for tensile stresses normal to the {100} planes.

Other investigators[17] had likewise found evidence of kinking in several ionic crystals of the rock salt structure, due to intersection of slip bands during plastic deformation.

C. Deformation at Different Temperatures

Studies of TlI-TlBr mixed single crystals deformed at different temperatures and rates showed that there was a substantial change in the range of plasticity (the yield strength and extent of deformation). At sufficiently low deformation rates, the range of plasticity varied about a hundred-fold with a temperature change from 20 to 250°C. This indicated that the basic deformation process was a function of temperature.[18] This study was confirmed by Regel and Tomilovskii,[19] who investigated the temperature and time response of the glide process. These researchers found that the temperature response of the creep strength remained insignificant at low temperatures up to medium temperatures, but that the creep strength was sharply reduced when melting temperatures were approached.

The previous data indicated that a thermal activation process for glide which Regel and Tomilovskii suggested was contrary to the conclusion by Schmid and Boas.[20] Schmid and Boas assumed that the basic process of glide was athermal and did not depend either on the temperature or the deformation rate. They felt that the role of the temperature was to soften the crystal through an increase of lattice vibrations, which effect was superimposed on the basic athermal process.

D. Some Characteristics of Polycrystalline Aggregates

Plastic deformation in polycrystalline aggregates requires that the material and the stress remain continuous throughout the aggregate.[9] The requirement of continuity of the material, or the requirement that gaps do not form at the grain boundaries, requires slip to take place on

at least five different slip systems if the volume per grain remains constant.[21] The orientation of a polycrystalline material is such that the necessary applied stress needs to be very high to cause some of the slip systems to function. In fact, some other mechanism of deformation may have to be activated, such as twinning kinking, or cross-slip, to satisfy the condition of the functioning of at least five different slip systems. (Cross-slip is the process in which a screw dislocation glides out of its slip plane onto another plane.) The requirement of continuity of stress means that the stress in each grain is not independent of the stress in the other grains.

Recent investigations[22] of polycrystalline ceramics of the rock salt type of structure showed that above a certain temperature the material deformed plastically and fractured in a ductile manner, while below this temperature the material possessed some ductility but failed in a brittle fashion. The explanation of this behavior was that easy cross-slip set in above the transition temperature. This provided an additional means of deformation within the grains. The transition temperature seemed to be in the vicinity of one-half of the melting point on the absolute temperature scale. If the temperature was too high, the mode of fracture changed from transgranular cleavage (through the grains) to an intergranular mechanism (grain boundary separation), which resulted in a reembrittlement of the polycrystalline material. Stokes and Li[4] felt that this was due to the extreme weakness of the intergranular shear strength of ionic solids above one-half of the melting point, as shown by Adams and Murray.[23]

III. EXPERIMENTAL PROCEDURE

A. Single Crystals

Cut cesium bromide single crystals were obtained from the Harshaw Chemical Company for these experiments. The crystals were first annealed at 500°C for two hours in a vacuum of 1μ Hg, then were cooled to 200°C in three hours.

Specimens of known orientation were made from the annealed single crystals for tensile, bending, and compressive tests. The single crystals were oriented with the aid of Laue x-ray diffraction patterns. These patterns revealed some substructure in the cesium bromide, which may have had some effect on the mechanical behavior as noted later.

As cesium bromide is soluble in water, the crystals were dry cut into specimens by a diamond saw at the proper orientations. The single crystal specimens were water-polished, prior to testing, by rubbing the surfaces with a soft tissue soaked with distilled water. The surfaces of specimens to which compressive loads were to be applied were sanded parallel to each other in a special holder to ensure application of uniformly applied loads.

The single-crystal tensile tests at room temperature were performed on the machine shown in Fig. 1. This machine did not rigidly fix the specimen in position. The specimens were mounted in steel grips with an epoxy resin glue, allowing a 1/2-in. gauge length. Tensile tests were performed at various temperatures on an Istron Universal testing machine with the apparatus shown in Fig. 2. The bending tests were performed on the Instron with the aid of a four-point loading jig, with the upper span equal to 0.75-in. and the lower span equal to 0.25 in. The displacement rates were 0.002 in./min and 0.005 in./min for the tensile and bending tests, respectively. The compression tests at room temperature were performed on the Instron at a constant displacement rate of 0.005 in./min. Compression tests were also run at 300°C at a constant rate of loading. The stresses were calculated on the

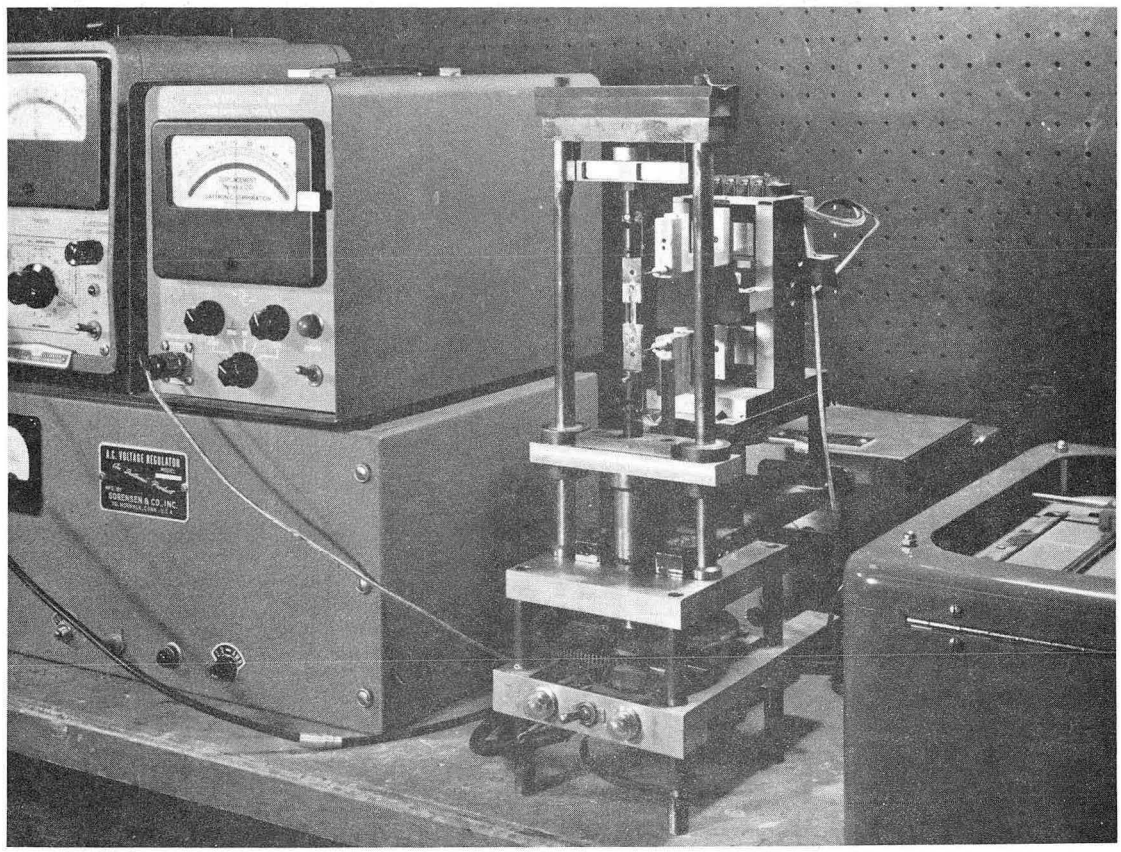

ZN-3410

Fig. 1. Tensile-test apparatus.

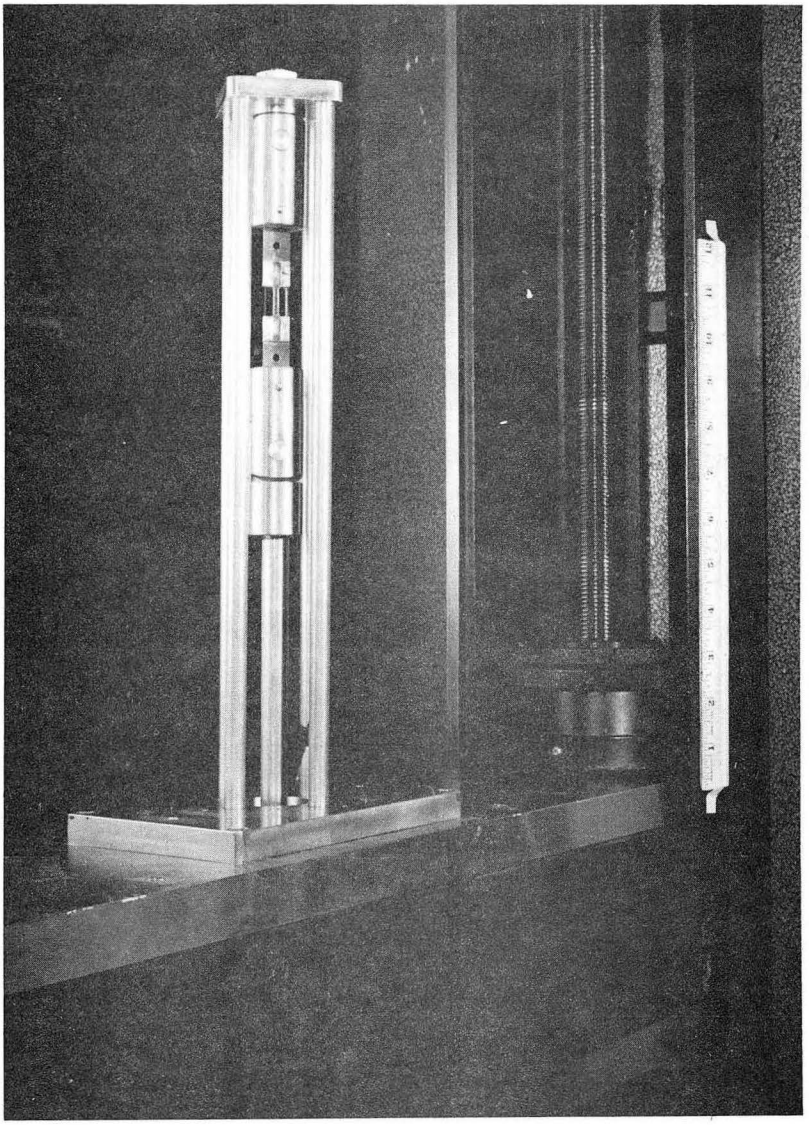

ZN-3411

Fig. 2. Apparatus for tensile testing on Instron machine.

basis of the initial cross-sectional area, and strains on the basis of the original gauge length.

An etchant was not developed, but slip traces were visible after deformation on the surfaces of the polished specimens and also under polarized light.

B. Polycrystals

Polycrystalline cesium bromide disks were made under pressure in a steel mold in a number of ways: (1) a < 325-mesh (less than 325-mesh) powder pressed at 50,800 psi at 24°C in air, (2) a single crystal pressed at 50,800 psi at 24°C in air, and (3) a single crystal pressed at 8000 psi at 300°C in 0.2 μ Hg pressure, heated to 400°C under pressure and cooled to 100°C in 30 min. The disks were 1-1/4, 1-1/4, and 1 in. in diameter, respectively. The powdered compact and single crystal pressed at 24°C were translucent as they approached theoretical density, while the hot-pressed compact was almost completely transparent. The material for the < 325-mesh powdered compact was obtained from the single-crystal scraps, purified by a zone refining process with the aid of a furnace developed by Scott,[1] and ground to a < 325-mesh size inside a glove box by using a diamonite mortar and pestle. The material to be purified was lowered through the furnace at a rate of 1/2 in./h in a natural temperature gradient, with the maximum temperature at 700°C. The material was usually clear after two or three runs. Purification of the cesium bromide before grinding was necessary because the material was easily contamiated and hygroscopic. The glove box, which contained a helium atmosphere, also helped reduce the impurity content in the powdered compact. The procedure of pressing single crystals to form large-grained polycrystalline material should have eliminated the possibility of occluded gases or impurities at the grain boundaries, as compared to pressing the cesium bromide powder, which contained interstitial holes and possibly adsorbed gases.

After preparation, the polycrystalline disks were cut by a hacksaw into approximately 1- by 1/10-in. square specimens, and water polished by rubbing on soft tissue soaked with distilled water. The specimens for the tension tests were subsequently tested in the Instron, while the specimens for the bend tests were tested in four-point loading in a small Instron. The lower and upper spans of the bending jig were 3/4 in. and 1/4 in., respectively. The strain was calculated by

$$\text{strain} = h/2r, \tag{2}$$

where

$$r^2 = \Delta^2 + 5/64 + 1/256\,\Delta^2 \tag{3}$$

and h is the specimen height. The cross-head speed, Δ, was 0.01575 in./min. The stress was calculated by

$$\text{stress}_{max} = Mc/I = 12hw(\text{moment arm})/4bh^3, \tag{4}$$

where w is the load, b is the specimen breadth, and the moment arm was 1/4 in. The specimens for bending at 300°C were heated up to temperature in one hour in a small resistance-coil tube furnace which enclosed the bending jig.

IV. RESULTS AND DISCUSSION

A. Plastic-Deformation Behavior of Single Crystals

A theoretical investigation of the possible slip systems indicated that the six $\{110\}\ \langle 100\rangle$ systems would most probably be activated. The possibility of the activation of any other systems is remote because of the electrostatic forces within the crystal. The directions of slip, for instance, are limited to the $\langle 100\rangle$ directions because any other direction would reduce the distance between cations, thereby introducing repulsive forces within the lattice. Because of the direction of slip, glide can potentially occur on the $\{100\}$ and $\{110\}$ planes. Slip on $\{100\}$ planes is not expected, however, because such glide would cause an accumulation of ions of like sign at the step surfaces of the specimen.

The following investigation of single crystals is concerned with the mechanical behavior of the $\{110\}\ \langle 100\rangle$ slip systems which should appear for forces normal to various orientations of the single crystals. This investigation also compares the experimental behavior to that expected from theory. Slip on $\{100\}$ planes was not observed in any of the tests. The effect of the lack of cleavage is considered in the proposed mechanism of the mechanical behavior.

1. Calculation of Necessary Loads

Figure 3(a) shows the values of the applied shear stress for two $\{110\}\ \langle 100\rangle$ slip systems in cesium bromide for loads normal to any orientation within the triangle (see Appendix A for calculations). The orientation is represented by a loading direction that is indicated by the extension of any point within the triangle through the origin of the axis. The triangle represents the (111) plane of the crystal, and the axis is the crystallographic axis of the crystal. The lines within the triangle are contour lines of the reciprocal of the function $\cos\theta \cos\lambda$ of Eq. (1) and, therefore, are proportional to the applied shear stress. The solid lines represent the values of the reciprocal of $\cos\theta \cos\lambda$ of the (110)

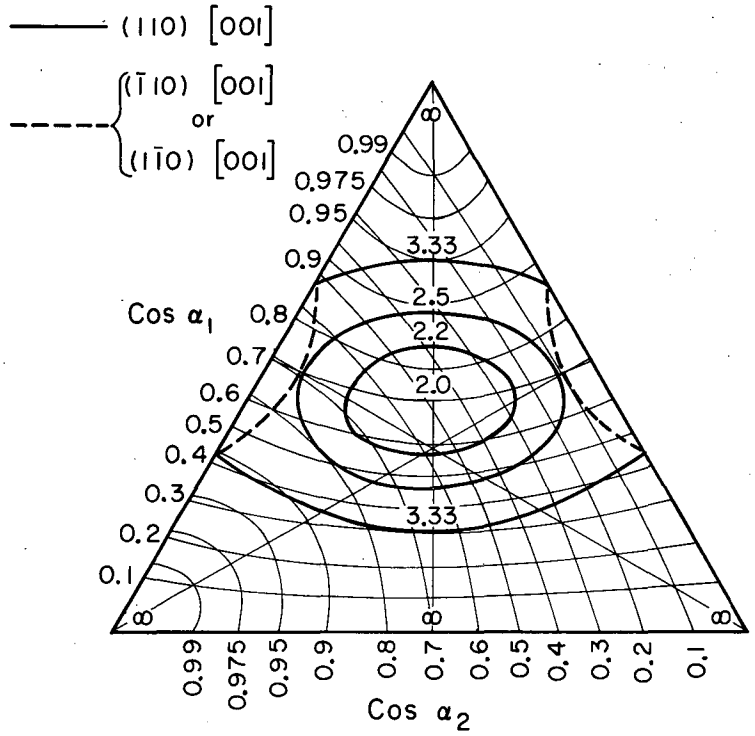

Fig. 3(a). A contour map of the resolved shear stress for any crystal orientation for two $\{110\}\ \langle 100\rangle$ slip systems.

[001] system; the dotted lines, of the equivalent $(\bar{1}10)$ [001] and $(1\bar{1}0)$ [001] systems. The values of the applied shear of the remaining four $\{110\}\ \langle 100\rangle$ systems are symmetrical to the first two in such a way that a 120° rotation of the triangle will duplicate the location of the contour lines. Figure 3(b) shows the applied shear stress of the most easily operated $\{110\}\ \langle 100\rangle$ slip system for any orientation. If the applied stress should become greater than that necessary to operate these preferred systems, then other $\{110\}\ \langle 100\rangle$ systems may also appear.

The orientations used in these experiments are shown in Fig. 4, where alpha, the angle between the tensile axis and the normal to the $(1\bar{1}0)$ plane, is varied from 0 to 90°. The theoretical applied stress necessary to activate each of the six slip systems for an angle alpha is shown in Fig. 5. The equations of the curves are derived in Appendix A on the basis of Eq. (1). The resolved shear stress is set equal to unity in the diagram, since it is assumed that identical resolved shear stresses are required to activate each of the six slip systems. The calculations for the indicated slip systems in Fig. 5 show that the applied stress is equal on four and infinite on one slip system for a load normal to the (110) plane (alpha equals 0°); the applied stress is equal on two and higher on three systems for loads from alpha equals 0 to 35.3°; the applied stress is equal on three and infinite on two systems for a load axis normal to the $(\bar{1}\bar{1}1)$ plane (alpha equals 35.3°); the applied stress is least on one and higher on four systems for alpha greater than 35.3°; and the applied stress is infinite on all systems for loads normal to the (001) plane (alpha equals 90°). The applied stress for the sixth slip system is infinite for all of these orientations. If the specimen is rigidly fixed in the machine so that the specimen is restrained from translating its ends, as in compression, slip will steadily become more difficult for the most favorable slip system and another system must operate, if sufficiently stressed, in order to maintain linear dependency. For example, Fig. 5 shows that the (110)[001] slip system is favored

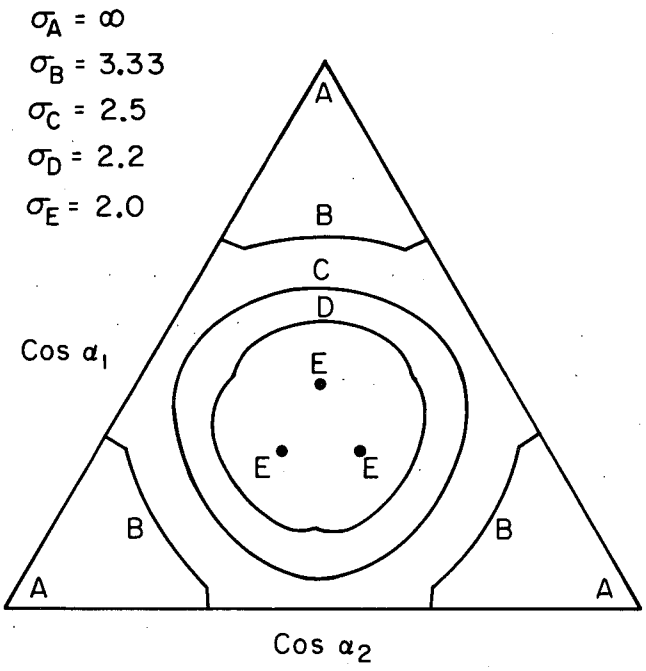

Fig. 3(b). A contour map of the applied shear stress for the most easily operated $\{110\}$ $\langle 100 \rangle$ slip system for any orientation.

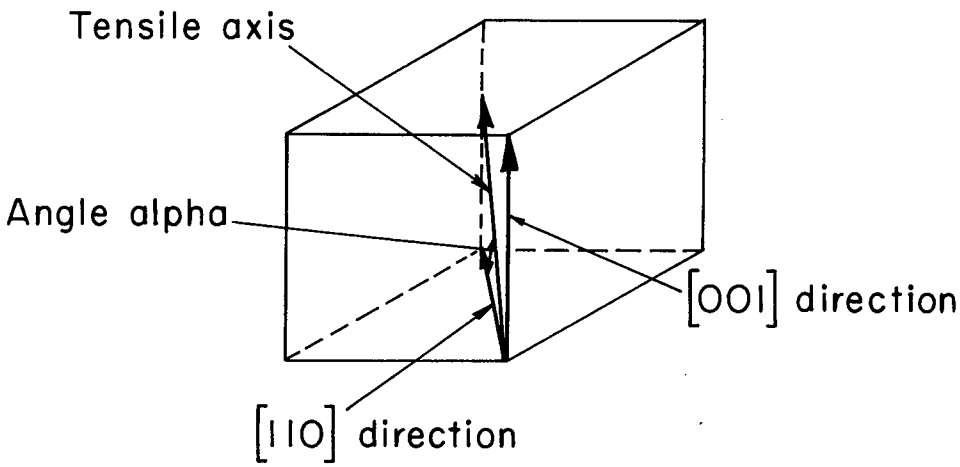

MU-28870

Fig. 4. Orientation of the tensile axis as a function of the angle alpha. Cube surfaces are {100} planes.

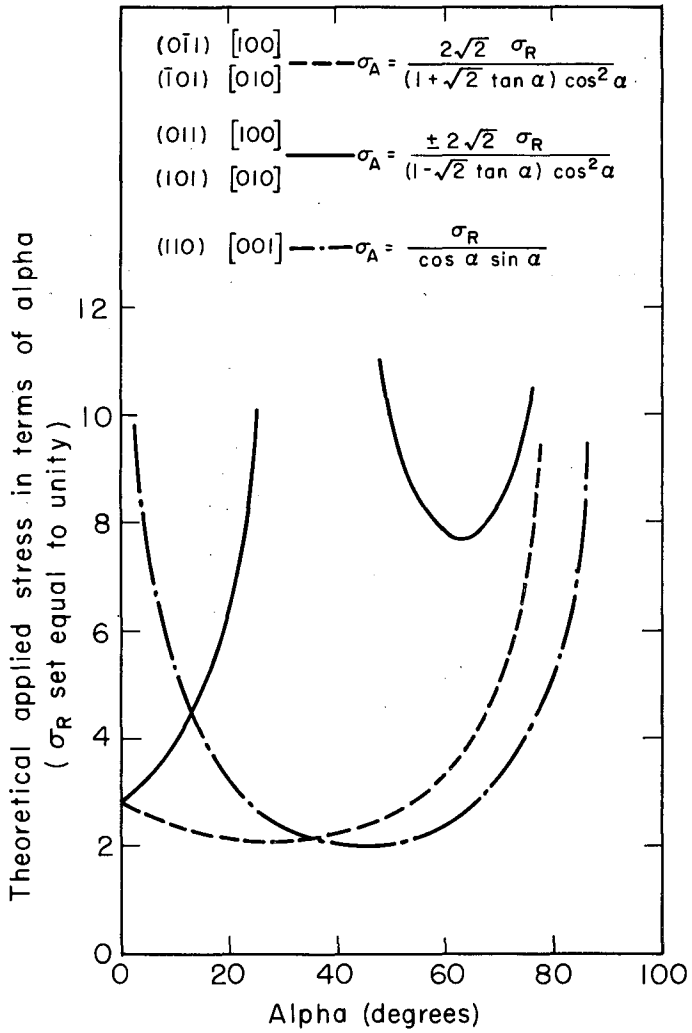

Fig. 5. Applied stress of the $\{110\}$ $\langle 100 \rangle$ slip systems as a function of alpha.

for alpha equal to 60°, but restrained slip may cause the $(0\bar{1}1)[100]$ and/or $(\bar{1}01)[010]$ slip systems to operate later.

2. Behavior in Tension

Figure 6 shows the stress-strain curves of cesium bromide specimens pulled at room temperature in the apparatus of Fig. 1, with alpha varying from 0 to 90°. The sample deformed in the 90° orientation exhibited a high stress level with little plastic flow, which is indicative of the absence of a resolved shear on any of the $\{110\}\ \langle 100\rangle$ slip systems, as shown theoretically in Fig. 5. The small amount of plastic flow observed could be explained by (a) a slight misorientation of the specimen, (b) the effect of very low-angle grain boundaries or subgrains as indicated in the x-ray Laue diffraction patterns, or (c) the formation of faults.

Figures 7 to 12 show photographs of slip traces appearing on the surfaces of the specimens, arranged according to the value of the angle alpha between the tensile axis and the normal to the (110) plane. The theoretical angles between the slip traces and specimen edge for each orientation are calculated in Appendix B. Neither slip traces nor any other traces appeared on the surface of the specimen for tensile forces normal to the (001) plane. Measurement of the angles of the slip traces with the specimen edge of Fig. 7(a) shows that the slip systems $(\bar{1}01)[010]$ and $(011)[100]$ appeared for the 0° orientation, as schematically shown in Fig. 7(b). When the tensile axis was shifted through 15° and 29°, then only the $(\bar{1}01)[010]$ system appeared, as shown by Figs. 8 and 9. The dashed trace in Figs. 8b and 9b represents the missing $(0\bar{1}1)$ trace, which should have appeared as indicated in Fig. 5. When the tensile axis is approximately normal to the $(\bar{1}\bar{1}1)$ plane (35.3° orientation), then three slip systems of the $\{110\}\ \langle 100\rangle$ type appeared, as shown in Fig. 10. The $(0\bar{1}1)[100]$ slip system (the heavy line in Fig. 10b) dominated the deformation process, while the remaining two systems also appeared near the grips. The photographs of Fig. 10, incidentally, were taken near the grips. For angles of 44° and 62°, the $(110)[001]$ slip system appeared as shown by Figs. 11 and 12.

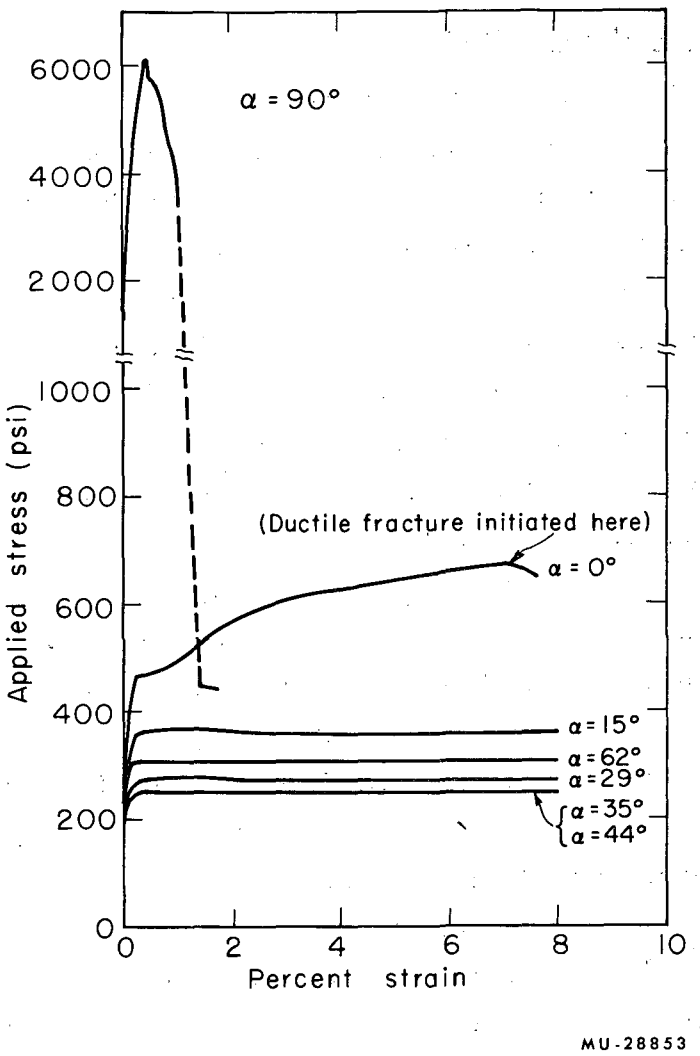

Fig. 6. Stress-strain behavior in tension of cesium bromide single crystals of different orientations of alpha at 24°C.

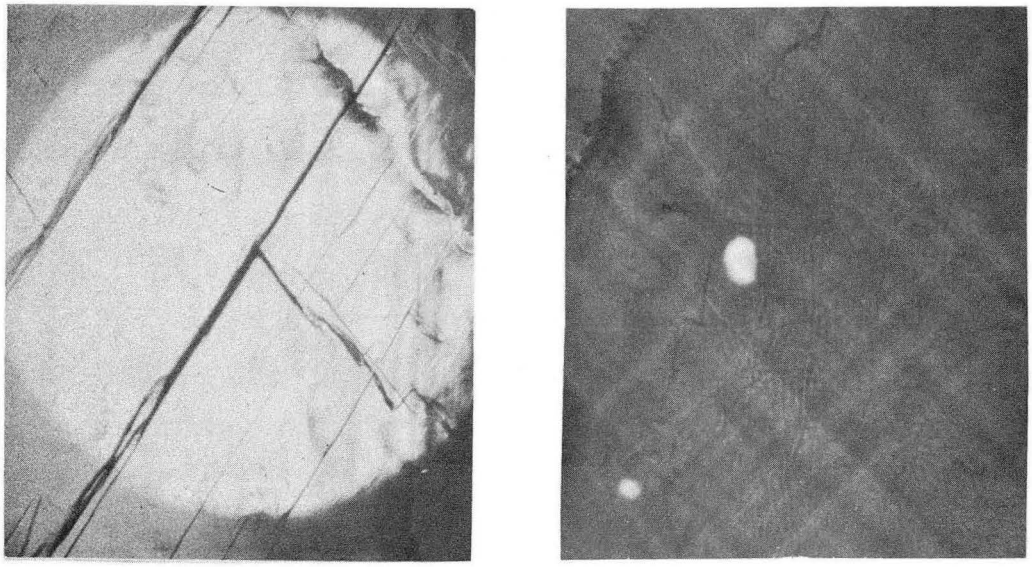

($\bar{1}10$) face, 100×, polarized light

(001) face, 150×

(a). ($\bar{1}01$) and (011) slip traces.

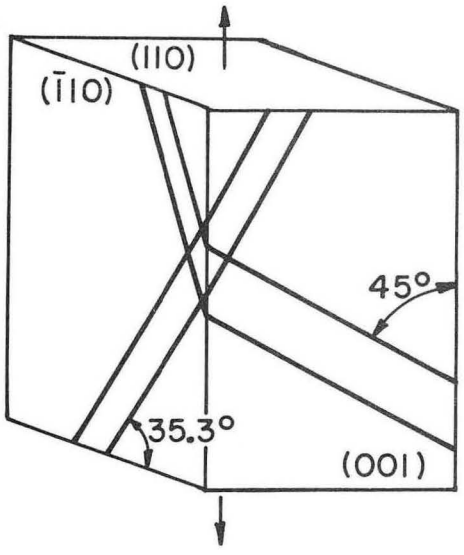

(b). Schematic mode of deformation for the ($\bar{1}01$) and (011) slip traces.

Fig. 7. Deformation in cesium bromide for the 0^0 orientation.

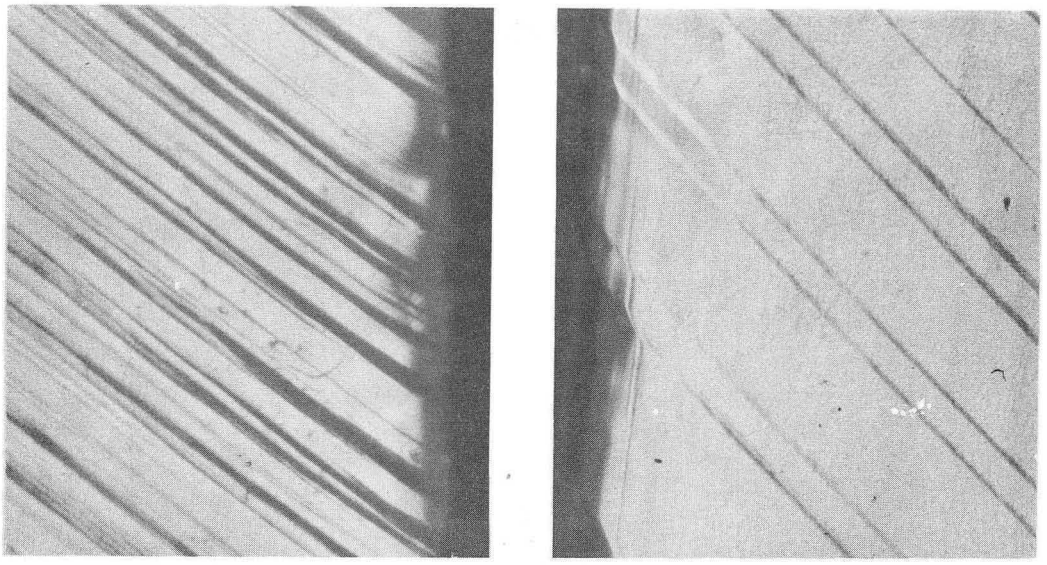

($\bar{1}10$) face, 150× $\alpha = 15^0$ face, 150×

(a). ($\bar{1}01$) slip traces.

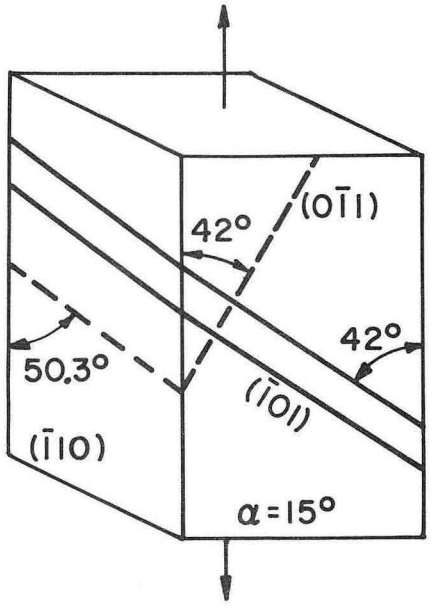

(b). Schematic mode of deformation for the ($\bar{1}01$) slip trace. (Dashed line is the missing ($0\bar{1}1$) trace.)

Fig. 8. Deformation in cesium bromide for the 15^0 orientation.

ZN-3414

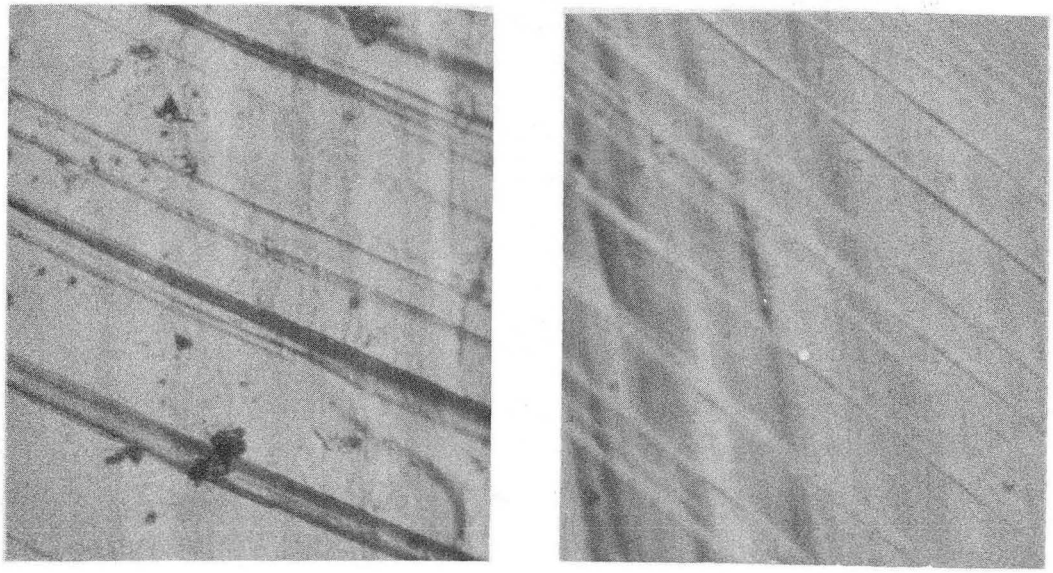

($\bar{1}10$) face, 150X $\alpha = 29^0$ face, 150X

(a). ($\bar{1}01$) slip traces.

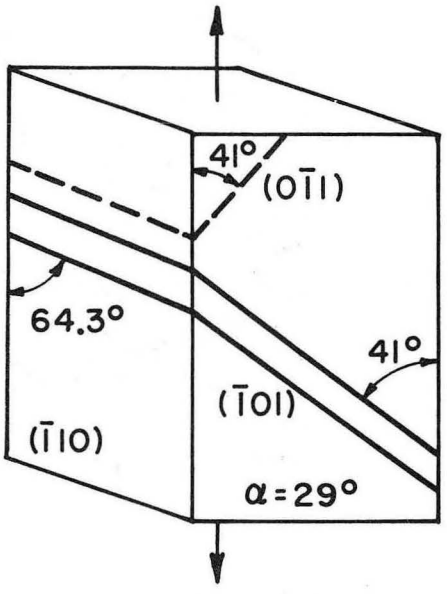

(b). Schematic mode of deformation for the ($\bar{1}01$) slip trace. (Dashed line is the missing (0$\bar{1}$1) trace.)

Fig. 9. Deformation in cesium bromide for the 29^0 orientation.

ZN-3415

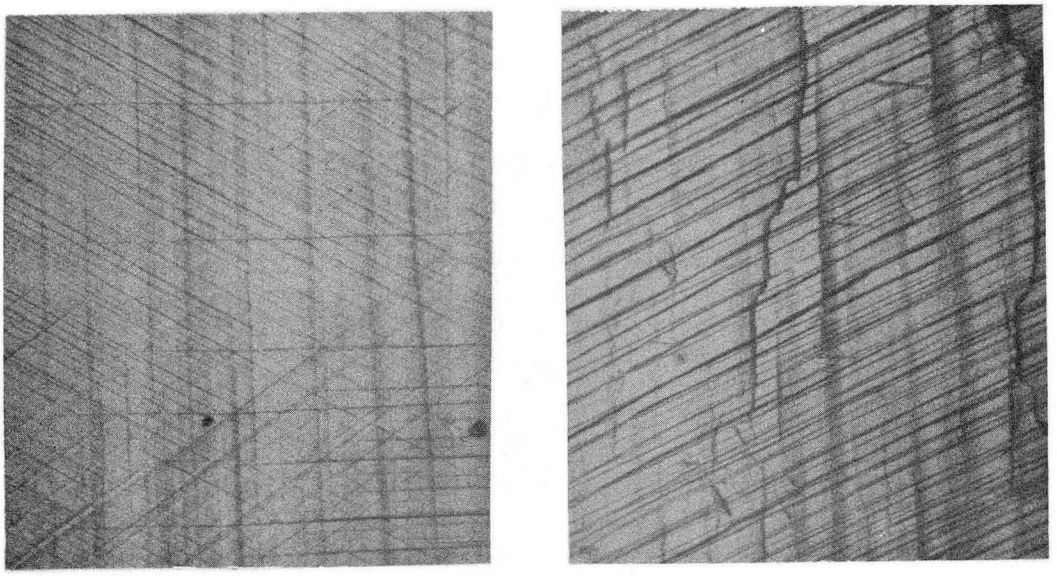

(112) face, 150× ($\bar{1}$10) face, 150×

(a). (0$\bar{1}$1), ($\bar{1}$01), and (110) slip traces.

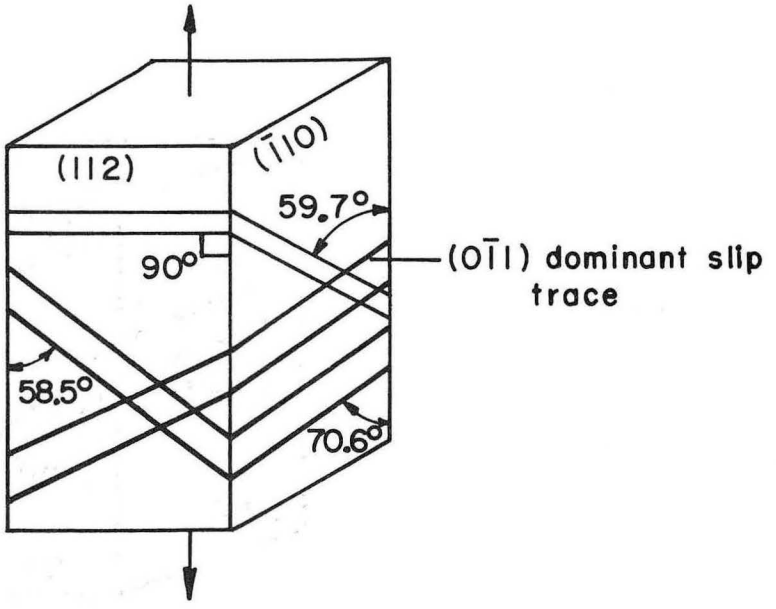

(b). Schematic mode of deformation for (0$\bar{1}$1), ($\bar{1}$01), and (110) slip traces.

Fig. 10. Deformation in cesium bromide for the 35° orientation.

ZN-3416

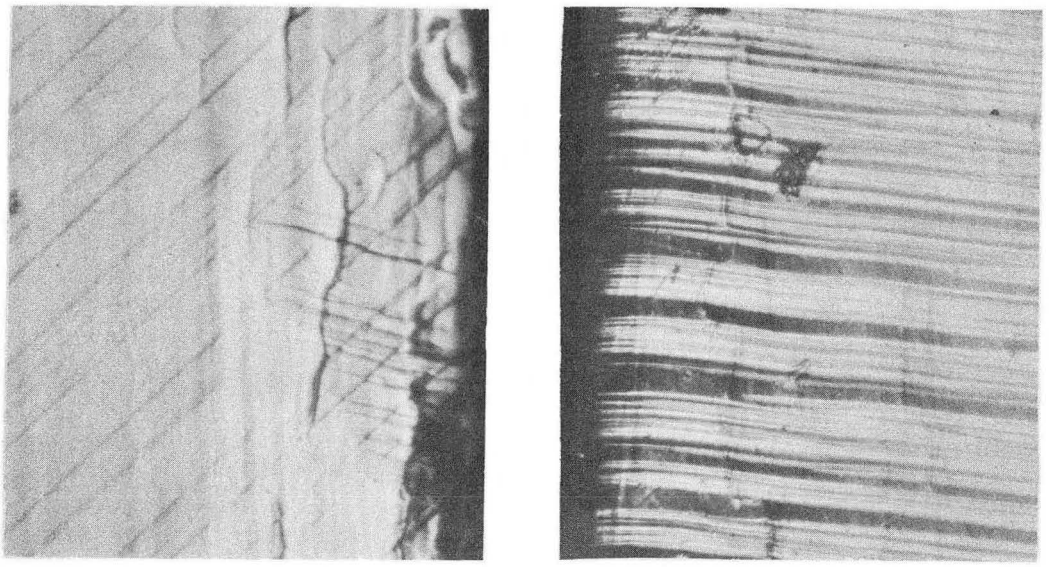

($\bar{1}10$) face, 150X $\alpha = 44^0$ face, 150X

(a). (110) slip traces.

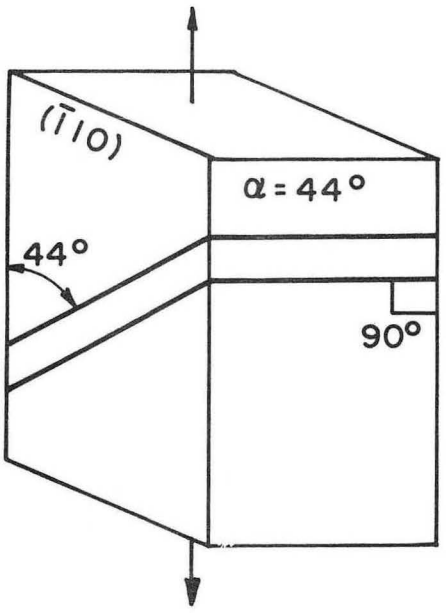

(b). Schematic mode of deformation for (110) slip trace.

Fig. 11. Deformation in cesium bromide for the 44^0 orientation.

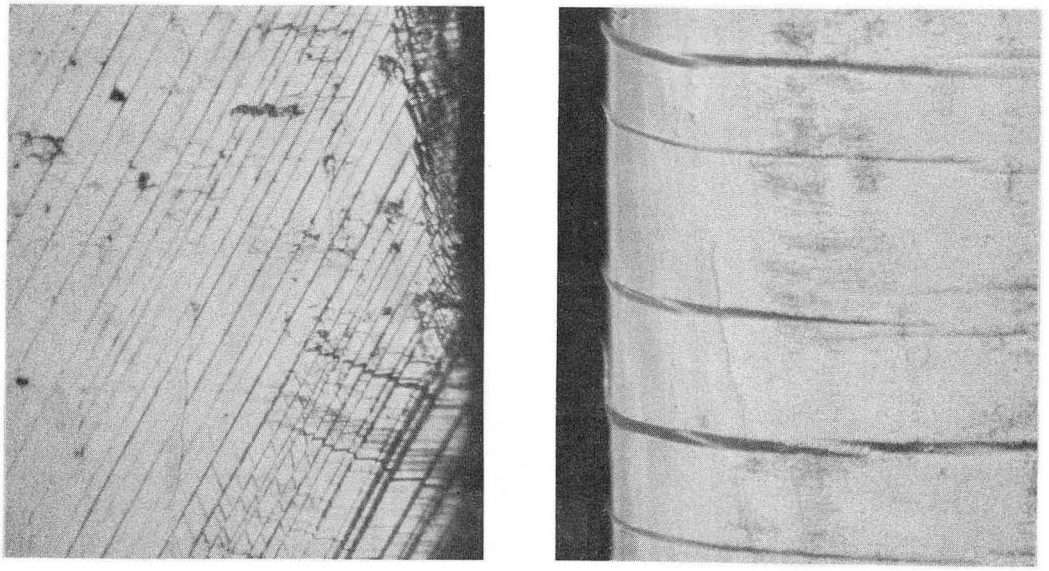

($\bar{1}10$) face, 150X $\alpha = 62^0$ face, 150X

(a). (110) slip trace.

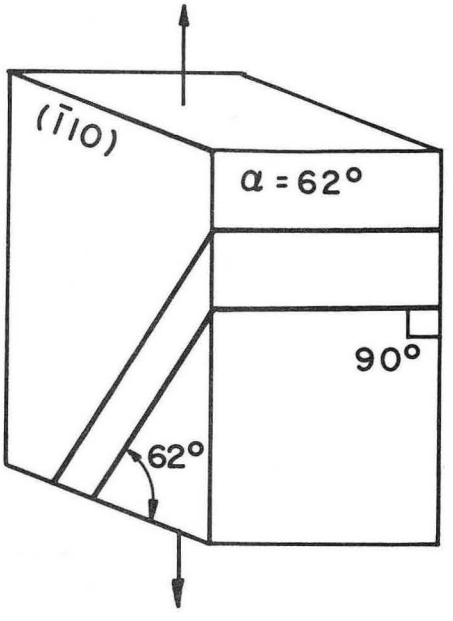

(b). Schematic mode of deformation for (110) slip trace.

Fig. 12. Deformation in cesium bromide for the 62^0 orientation.

3. Discussion of the Behavior in Tension

The appearance of the slip traces in Figs. 7 to 12, on the basis of the lowest resolved shear stress and the use of a machine with non-rigid jigs, coincides with the theoretical prediction of Fig. 5 except that four instead of two systems should have appeared for alpha equals 0°, and two instead of one for alpha equals 15° and 29°. The difference between the theoretical and experimental picture can be attributed to the inherent dislocation forces. Figure 13 shows the direction of the Burger's vectors for each of the slip systems that should appear for the 0° orientation. Part (a) of the figure shows that slip planes that intersect at 60° angles have their Burger's vectors at 90° to each other; part (b) shows that the slip planes that intersect at 90° angles have parallel Burger's vectors. The parallel Burger's vectors are also of the same sign (same direction) because of the singular vector of the shear stress. Cottrell[9] showed that dislocations with Burger's vectors at 90° to each other have no interaction forces between them, while repulsive forces are incident on screw dislocations of the same sign (parallel Burger's vectors). In cesium bromide, therefore, deformation by slip on planes at 90° to each other is more difficult than deformation by slip on planes at 60° to each other. Slip on planes at 90° to each other may not occur at all if slip on planes at 60° to each other proceeds at a sufficiently low stress level, because of slight misalignment or possibly because of unrestrained ends. The two slip bands that appeared in the experimental results for the 0° orientation as shown in Fig. 7 intersected at 60° angles and their Burger's vectors were in the same plane with the loading direction. It will be shown later, through Fig. 19, that all four systems appeared in the specimen for a compressive load normal to the (110) plane, because in this case the forces necessary for translation of the ends of the specimen were greater in compression than in tension. Only one slip system appeared for the 15° and 29° orientations—probably because of a slight misalignment of the specimen or because of intersection difficulties accompanied

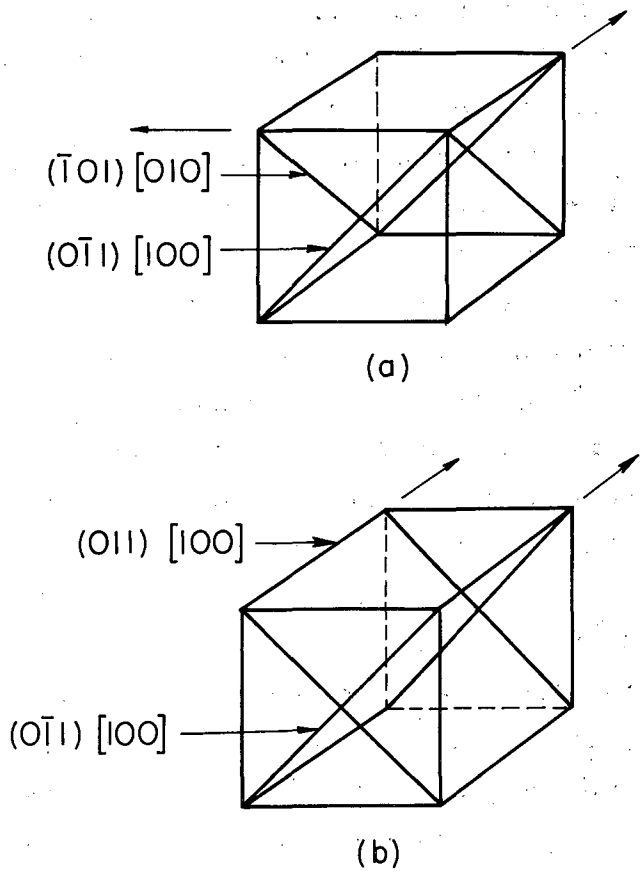

Fig. 13. Schematic illustration of Burger's vectors of the {110} ⟨100⟩ slip systems.
(a). 60° intersection of slip planes. Burger's vectors are perpendicular to each other, resulting in no repulsive forces. (Also similar for (011)[100] and (101)[010]).
(b). 90° intersection of slip planes. Burger's vectors are parallel and of same sign, resulting in repulsive forces. (Also similar for (1̄01)[010] and (101)[010]).

by unrestrained ends. The contour map in Fig. 3(b) shows that misalignment would result in a higher resolved shear stress on one of the two possible systems. Only one system would operate, therefore, until the load was sufficiently high to activate the second slip system or to force intersection. The appearance of only one slip system in the bulk of the specimen for the 35.3° orientation can also be explained on the basis of the same reasoning. Near the grips, however, the restraining forces were great enough to raise the resolved shear stress to activate all three systems—flow on all three systems being necessary to maintain linear dependency.

Work-hardening was found for the 0° orientation, but not for the other orientations, exclusive of the 90° orientations, exclusive of the 90° orientation, as shown in Fig. 6. Work-hardening occurs in a specimen when an increasing stress is required to make the specimen deform after the yield stress has been reached. Figure 7 shows that two intersecting slip systems operated for the 0° orientation; Figs. 8, 9, and 11 show that only one slip system operated in these specimens. The left side of Figs. 10(a) and 12(a) also exhibit other systems that produced local work-hardening, but these did not interfere with the activation of the dominating (110) [001] slip system. Figure 10 shows that three slip systems operated, but the $(0\bar{1}1)$ [100] system dominated during deformation. These results therefore provide evidence that the work-hardening found in the 0°-orientation specimen was caused by the intersection of two slip planes at 60° to each other. Intersections of these slip planes can cause work-hardening through the formation of jogs. A jog is a step in a dislocation line that is caused in this case by the passage of other dislocations. For the case of slip planes intersecting at 60° angles in cesium bromide, the intersection of two edge dislocations causes a segment (step) of edge dislocation on a { 100 } plane, as shown in Fig. 14(a). Glide of dislocations on a { 100 } plane is restricted, because such glide causes an accumulation of charge of one sign at the offset surface of the crystal, as shown later in Fig. 30(a).

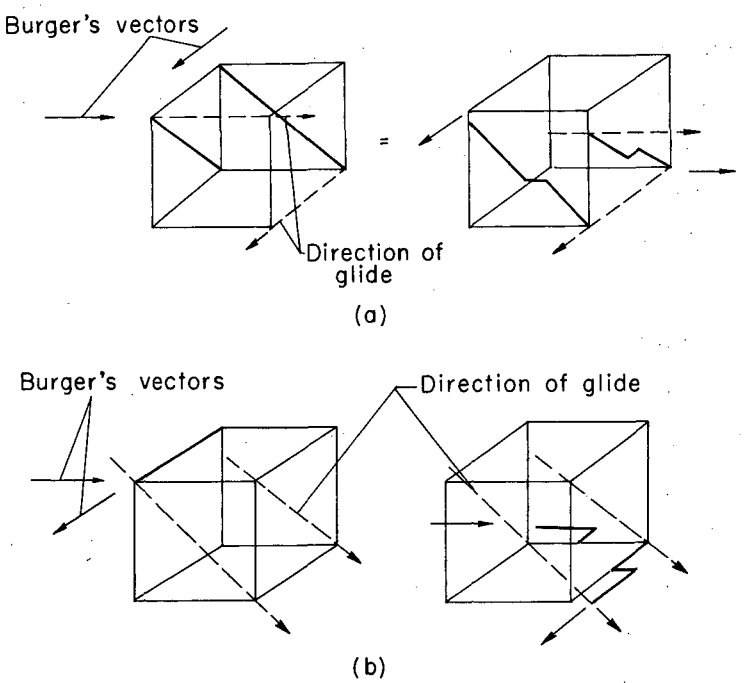

Fig. 14. Formation of jobs in dislocations of the {110} ⟨100⟩ slip systems intersecting at 60° angles.
(a). Intersection of edge dislocations to form jogs on a {100} plane.
(b). Intersection of gliding screw dislocations to form jogs on a {100} plane.

The intersection of two screw dislocations likewise causes segments (steps) of edge dislocations on {100} planes, as shown in Fig. 14(b). The steps created in the screw dislocations seriously hinder the glide of the screws, because the edge-dislocation steps cannot glide with the screws. Edge dislocations can only move in the direction of their Burger's vectors unless the dislocations climb.

The appearance of only one slip system during straining made it possible to calculate the resolved shear stress required to cause one of the systems to slip. The average value of the resolved shear stress at the start of deformation was about 126 psi, as calculated from the data and formulas in Fig. 5. The yielding effect in the stress-strain curves for the 15^{o} and 29^{o} orientations, in Fig. 6, during initiation of slip (the hump in the curves) was probably caused by the nucleation or multiplication of dislocations.

4. Behavior in Bending

Figure 15 shows load-deflection curves of specimens deflected on (112), ($\bar{1}$10), and (001) planes. The load was considerably higher for bending on (001) planes compared with the other planes; the drop in stress was caused by the growth of cracks which had nucleated on the tensile surface directly over one of the pins.

Fugre 16 shows photographs and schematic modes of slip traces of the three slip systems which existed simultaneously for deflections normal to the ($\bar{1}$10) and (112) planes. The (110)[001] slip system also appeared on the ($\bar{1}$10) surface under polarized light. Figure 17 shows photographs of {110} slip traces on specimens deflected on a (001) plane, as illustrated schematically in Fig. 17(c). There was no evidence of other slip systems. The small deflection and high load indicated low resolved shear stress for this system.

5. Discussion of the Behavior in Bending

The load-deflection curves, as shown in Fig. 15, for loads normal to the ($\bar{1}$10) and (112) planes are the same, as they should be,

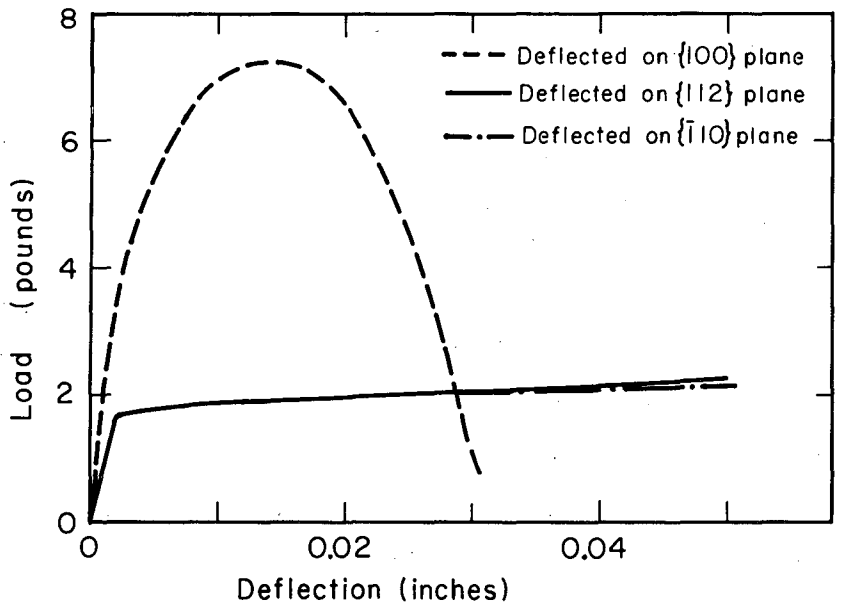

Fig. 15. Load-deflection curves for cesium bromide single crystals at 24°C.

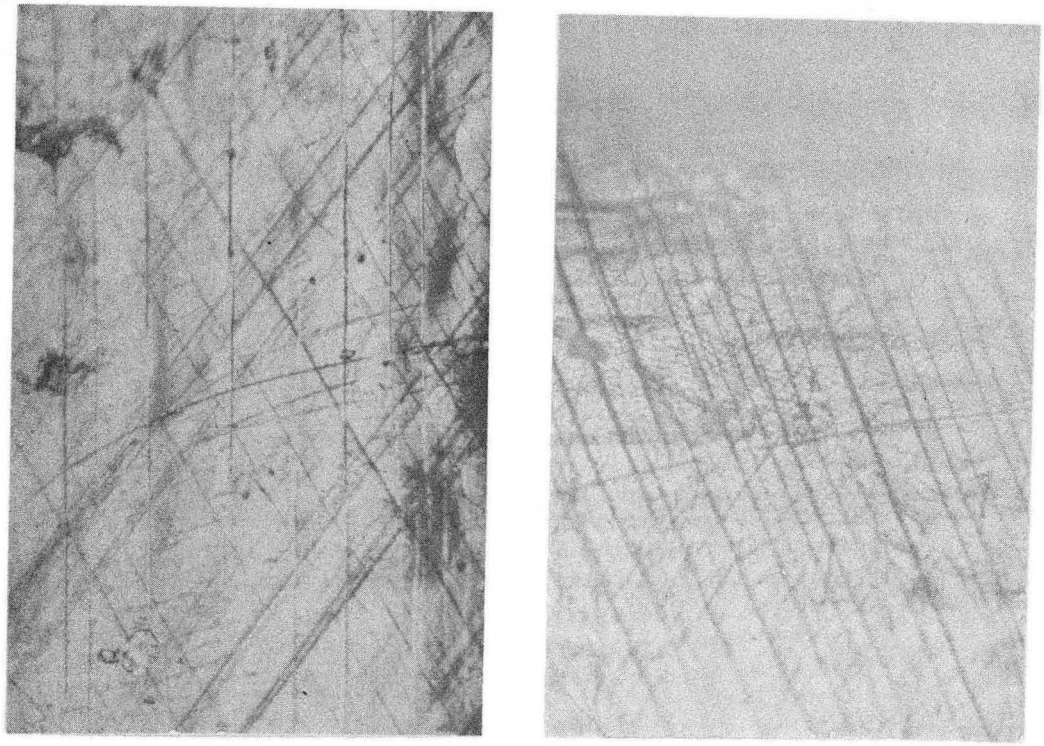

(112) face, 150X ($\bar{1}10$) face, 150X

(a). ($0\bar{1}1$), ($\bar{1}01$), and (110) slip traces.

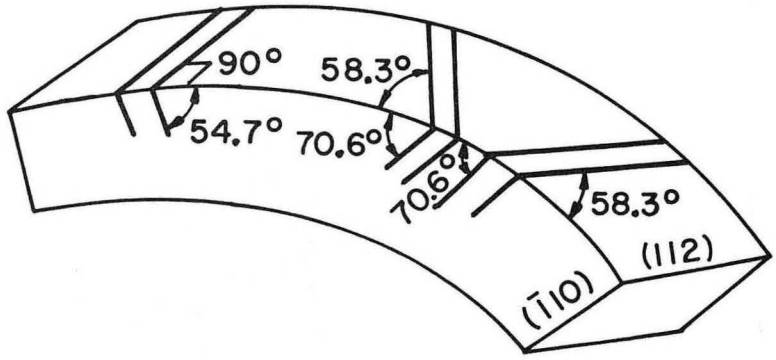

(b). Schematic mode of deformation for ($0\bar{1}1$), ($\bar{1}01$), and (110) slip traces.

Fig. 16. Deformation for bend specimen deflected on (112) plane.

ZN-3419

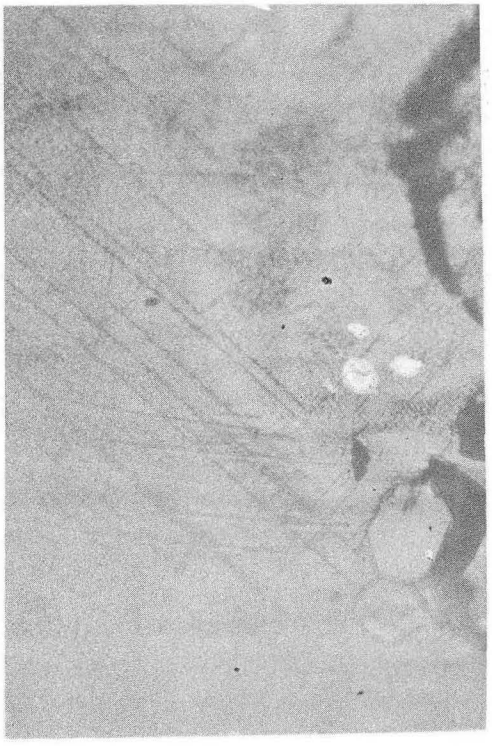

(a). (010) side surface.

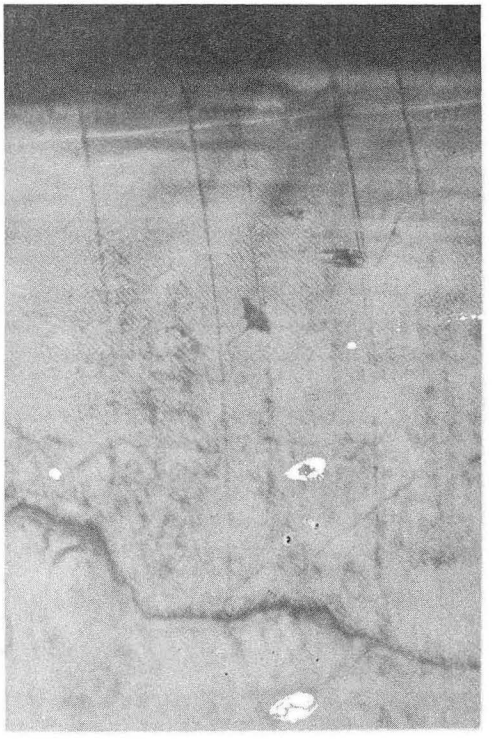

(b). (100) compression surface.

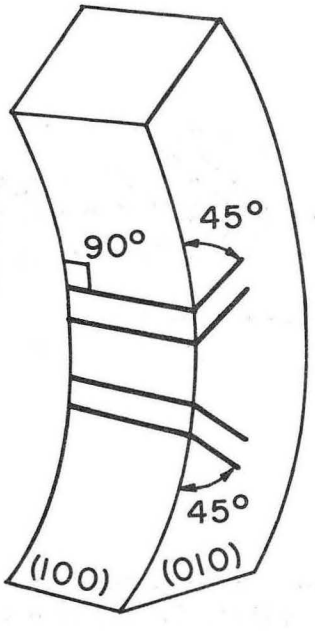

(c). Schematic mode of deformation for $(\bar{1}0\bar{1})$ slip traces.

Fig. 17. Deformation for bend specimen deflected on (001) plane.

ZN-3420

for equal-sized specimens, because the effective stresses were normal to the $(\bar{1}\bar{1}1)$ plane in both cases. Also, Fig. 16 shows that three slip systems appeared as predicted in Fig. 5 for this particular orientation. The load-deflection curve for loads normal to the (001) plane should exhibit only elastic behavior, at least at the beginning of loading, because a resolved shear stress did not exist on the $\{110\}\langle 100\rangle$ slip systems. The appearance of some plastic flow in the curve indicates misorientation of the specimen, which resulted in some glide as shown in Fig. 17. The observed glide, however, could also have occurred after some misalignment due to initial elastic bending of the specimens.

Work-hardening also existed for loads normal to the $(\bar{1}10)$ and (112) planes. This was probably due to intersections of the three slip systems to form dislocation jogs.

6. Behavior in Compression

Figure 18 shows the stress-strain curves for specimens with compressive loads normal to the (110), $(\bar{1}\bar{1}1)$, and (001) planes at 24°C. The curves for loads normal to the (110) and $(\bar{1}\bar{1}1)$ planes show considerable plastic deformation, compared to the curve for a load normal to the (001) plane. The curve for loads normal to the (001) plane shows little or no plastic flow accompanied by a high stress level and several load drops at the maximum stress level.

Figure 19 and the schematic diagram of Fig. 20 show that all four slip systems appeared for compressive loads normal to the (110) plane. The photographs in Fig. 19 indicate that two systems usually intersected each other in any particular area, except for the lower picture of Fig. 19(a) which shows three systems had intersected each other. Figure 21 shows the three slip systems that were activated for compressive loads normal to the $(\bar{1}\bar{1}1)$ plane.

Figures 22 and 23 show the surfaces of specimens for compressive loads normal to the (001) plane. These micrographs show that kinked areas, which had occurred suddenly, appeared and seemed to follow along indices of (11h) where h seemed to be about 4 and 8.

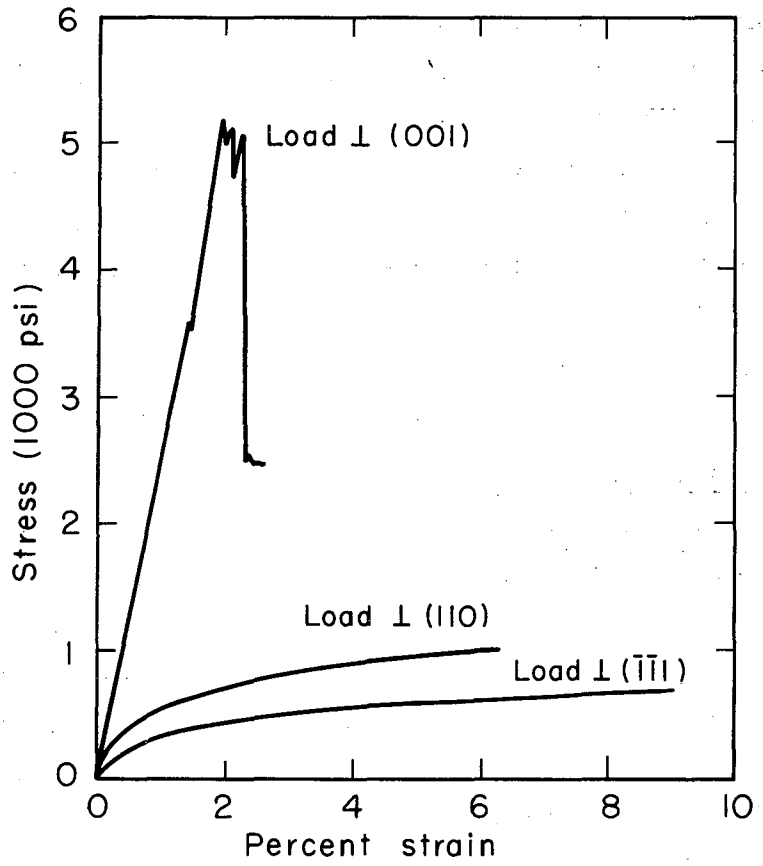

Fig. 18. Compression of cesium bromide single crystals at 24°C.

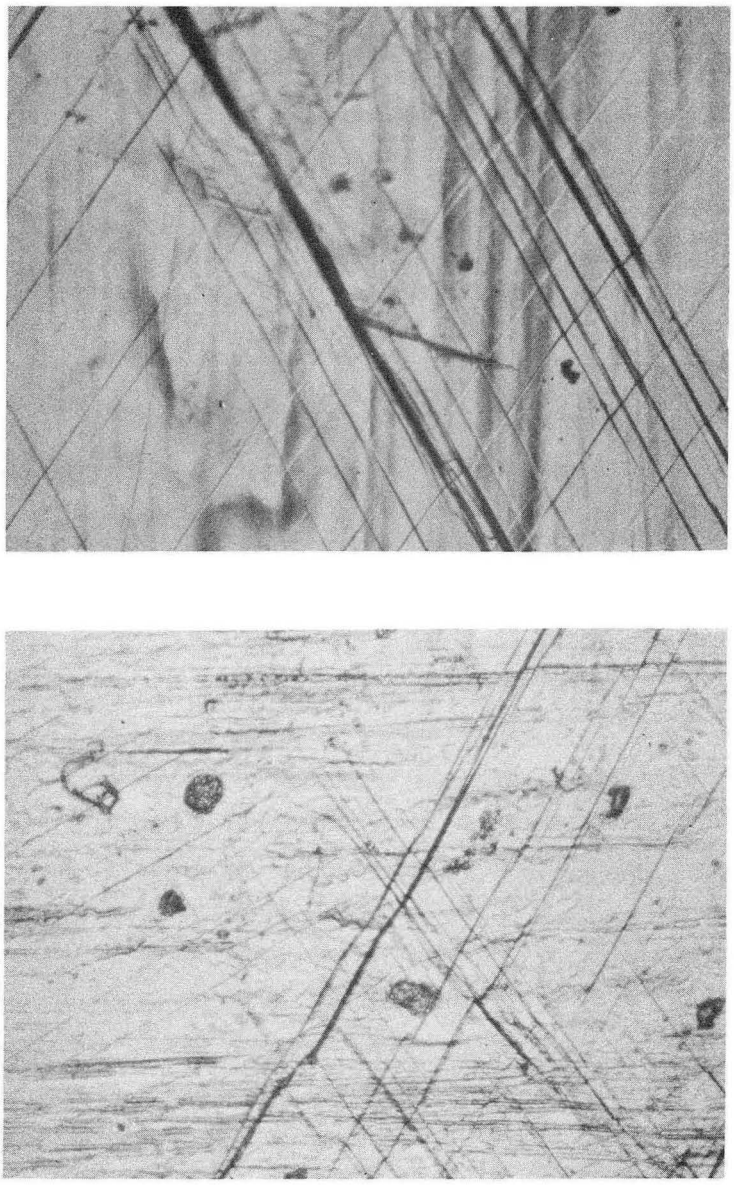

ZN-3426

Fig. 19(a). $(\bar{1}\bar{1}1)$ surfaces, viewing (011), (101), $(0\bar{1}1)$, and $(\bar{1}01)$ slip traces after compression loads normal to the $(\bar{1}10)$ plane at 24°C. 150X.

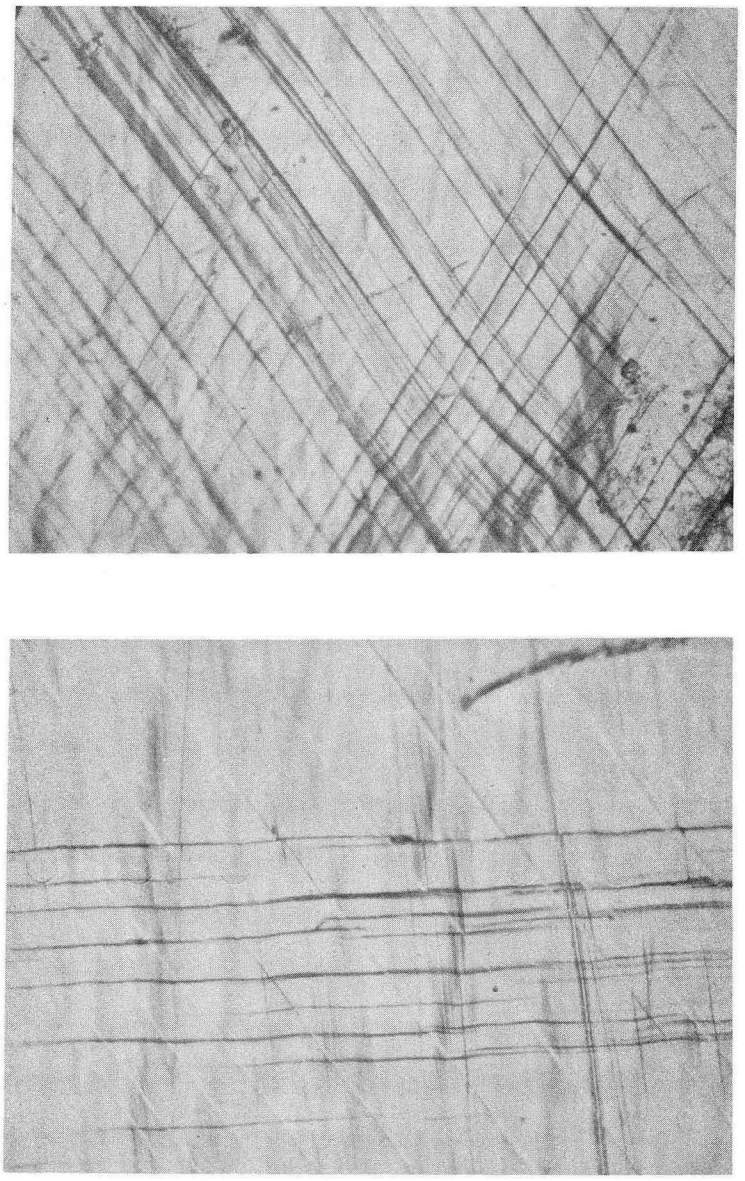

ZN-3427

Fig. 19(b). (112) surfaces, viewing (011), (101), (0$\bar{1}$1), and ($\bar{1}$01) slip traces after compression loads normal to the ($\bar{1}$10) plane at 24°C. 150X.

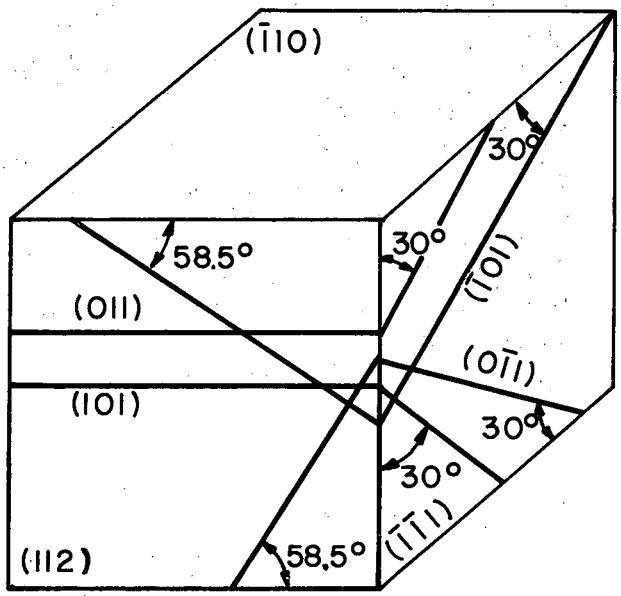

MU-28858

Fig. 20. Schematic mode of deformation for (011), (101), (01̄1), and (1̄01) slip traces shown in Fig. 19. The 30° angles on the (1̄1̄1) surface are calculated in Appendix III.

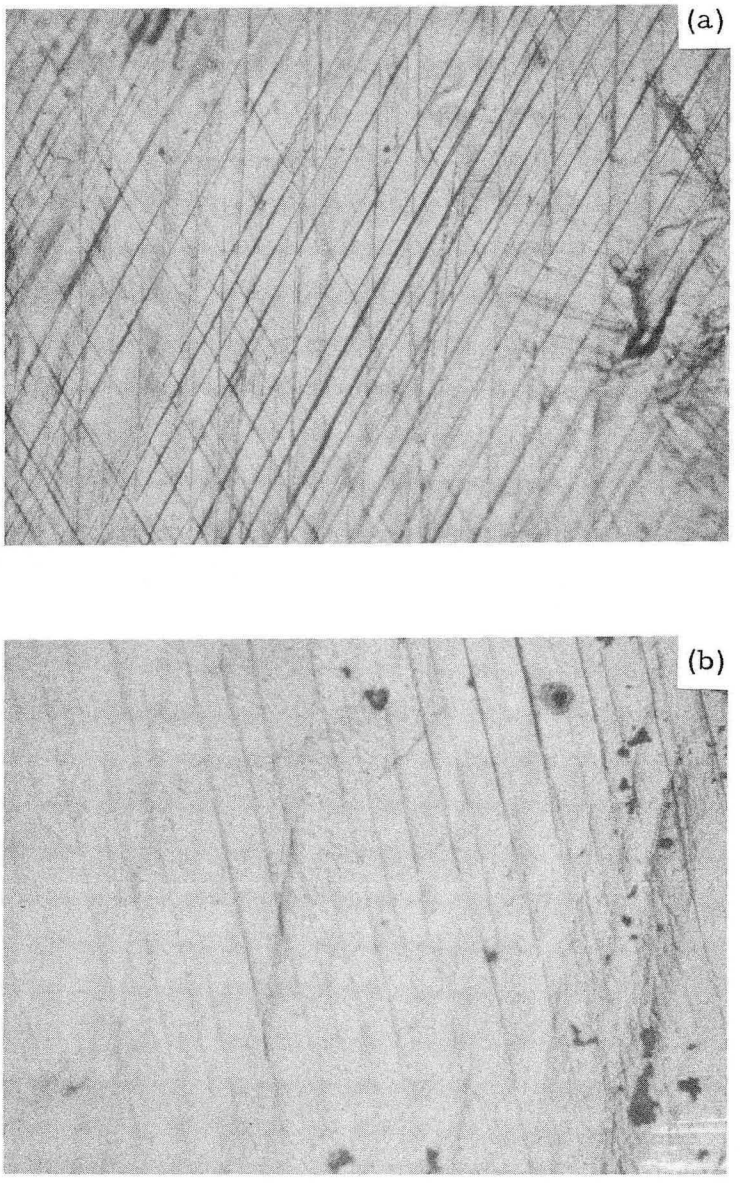

ZN-3428

Fig. 21. Adjacent surfaces of specimen: (110), (0$\bar{1}$1), and ($\bar{1}$01) slip traces after compression loads normal to the ($\bar{1}\bar{1}$1) face. 150X.
(a). (112) face.
(b). ($\bar{1}$10) face.

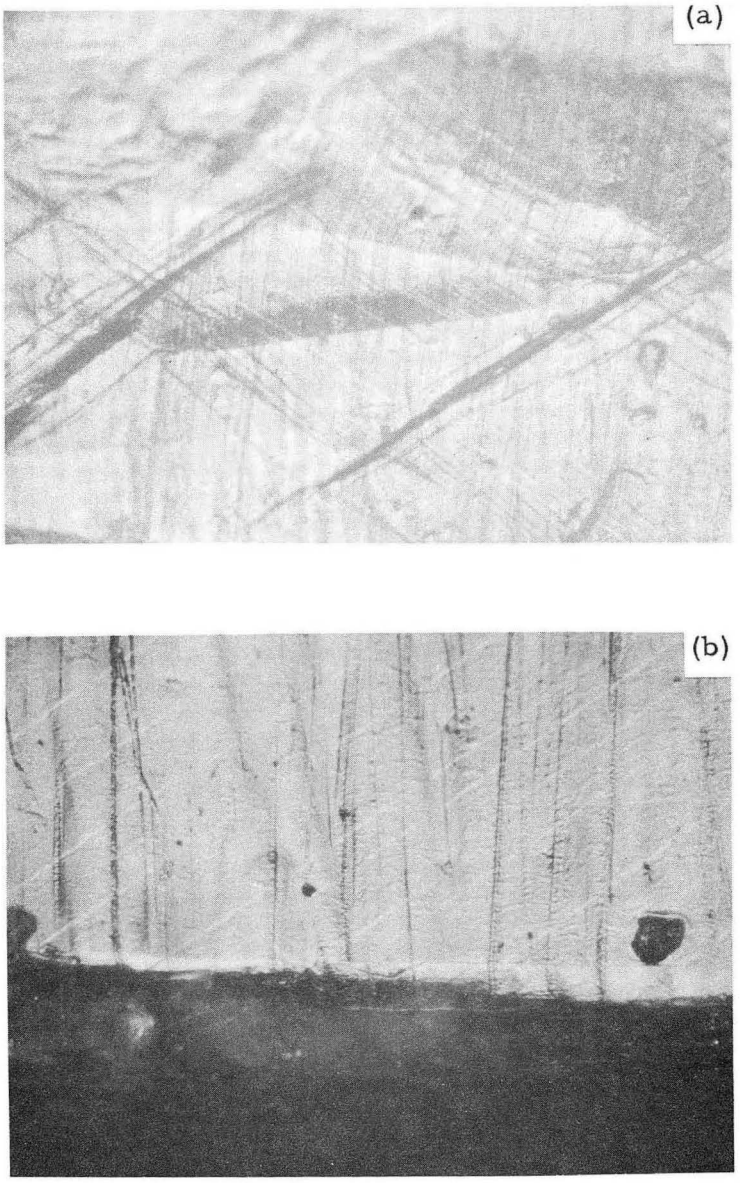

Fig. 22. Adjacent {110} faces after compression loads normal to the (001) plane at 24°C.
(a). (110) face, 75X.
(b). ($\bar{1}$10) face, 150X.

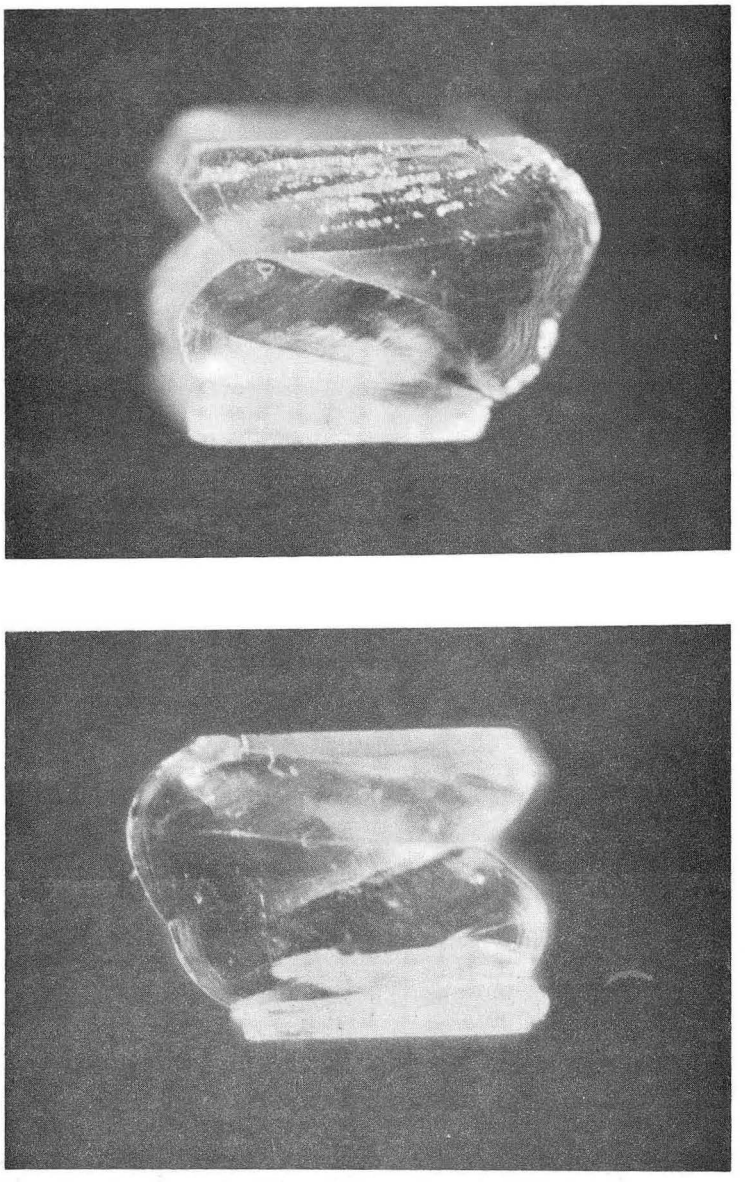

ZN-3430

Fig. 23. Opposite ($\bar{1}10$) faces after compression loads normal to the (001) plane at 300°C. 6X.

Figure 23 shows pictures at 6X of the kinks obtained at 300°C, which again appeared suddenly.

7. Discussion of the Behavior in Compression

A visual comparison of the tensile tests of Fig. 5 with the compressive tests of Fig. 18 is given in Fig. 24. The relative work-hardening rates between the tensile and compressive tests in the figure show that there was greater work-hardening in compression than in tension. Deformation by glide required the appearance of slip offsets at the surface of the specimen. This deformation usually translated the ends of the specimen if they were free to move. When the ends of the specimen could not move laterally during deformation, the slip planes had to rotate to compensate for the accumulation of slip offsets unless enough slip systems with properly oriented Burger's vectors operated to prevent the translation of the ends, i.e., the specimen was linearly dependent. During the current series of experiments, the ends of the specimens in the tensile tests could move laterally, hence glide did not cause the slip planes to rotate and the work-hardening due to this cause remained zero if only one slip system dominated the deformation process. Because the ends of the specimens in the compression tests were restrained from lateral motion, movement occurred on two of the four possible slip systems intersecting at 60° to each other for loads normal to a {110} plane and on all three systems for loads normal to a {111} plane, in order to maintain linear dependency of the slip systems for these orientations. Consequently, the work-hardening in compression was caused chiefly by the creation of jogs through dislocation intersections and by the friction forces at the steel plunger - cesium bromide interface rather than by rotation of the planes. The work-hardening in compression increased the stress sufficiently, in fact, to cause all four possible slip systems to operate for the 0° orientation, compared with the activation of only two of the four systems in tension. The difference between the linear portion of the curves before the yield in Fig. 24 for loads normal to the (001) plane was due, to some

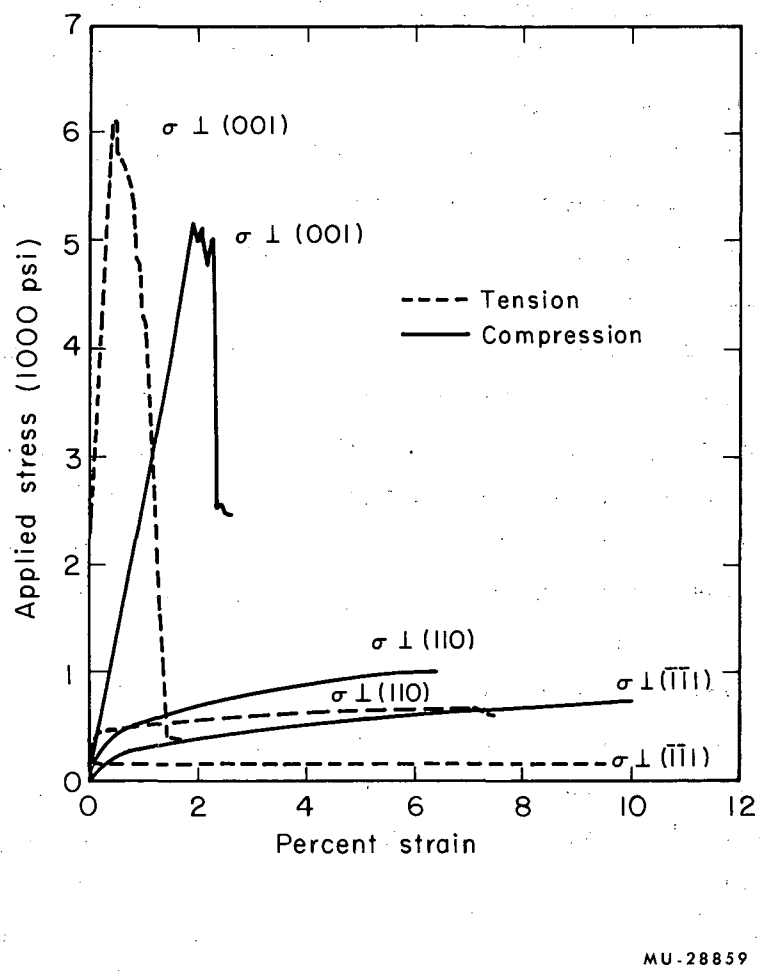

Fig. 24. Comparison of tension and compression tests at 24°C.

extent, to the relative softness of the compression-load cells of the Instron, compared with the apparatus of Fig. 1. Some plastic deformation may also have occurred at the steel plunger - cesium bromide interface before the yield was reached, thus altering the slope of the curve. Misalignment of the specimen and the difference in machines were further contributing factors to deviations between the two curves.

The wedge-shaped areas formed by compression loads normal to the (001) plane were characteristic of kink bands. Kolontsova and Telegina[13,14] argued that these kink bands could be formed through a twinning process. Twinning, however, would involve the existence of partial dislocations that are unstable in the cesium chloride structure because partial dislocations would force cations to be nearest neighbors. In other words, if the kink planes were actually twin planes, cations would have had to move into nearest-neighbor positions in order to form a mirror reflection of the lattice. On the other hand, kink bands consisting of numerous pure edge dislocations on the (110) planes in the [001] direction could quite easily be formed as shown in Fig. 25. The sharp lines of the bands could then consist of an array of edge dislocations of like sign. This suggestion explains very well the contours and the appearance of several apparent noncrystallographic bands in the specimens. Furthermore, jerky extension is characteristic of kinking.[11] The kink bands did not appear for tensile loads normal to the (001) plane, perhaps because fracture occurred first or the stresses were not complex as suggested to be necessary by Klassen-Neklyudova et al.[16]

8. Mechanism of Cross-Slip

Figure 26 shows photomicrographs of the surfaces of a specimen pulled normal to the $(\bar{1}\bar{1}1)$ plane at room temperature. These pictures show wavy lines on the $(\bar{1}10)$ face, indicating extensive cross-slip and a secondary cross-slip plane on the (112) face. Figure 27 shows examples of cross-gliding from one plane to another at 170°C, indicated by the arrows in the pictures, for a tensile load normal to the $(\bar{1}\bar{1}1)$ plane.

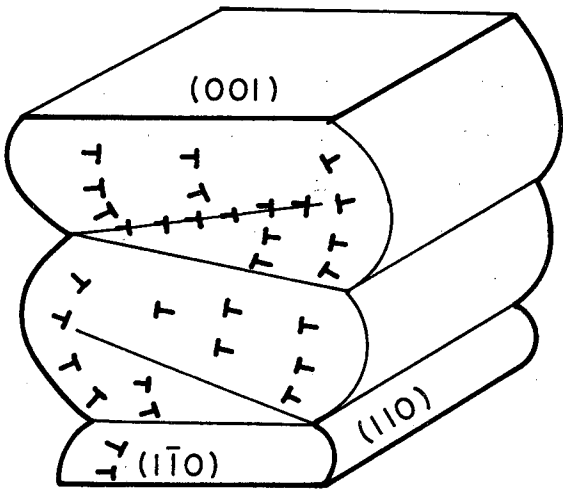

MU-28860

Fig. 25. Schematic illustration of pure edge dislocations gliding in the [001] direction on the (110) plane to form kink bands in the specimen of Fig. 23.

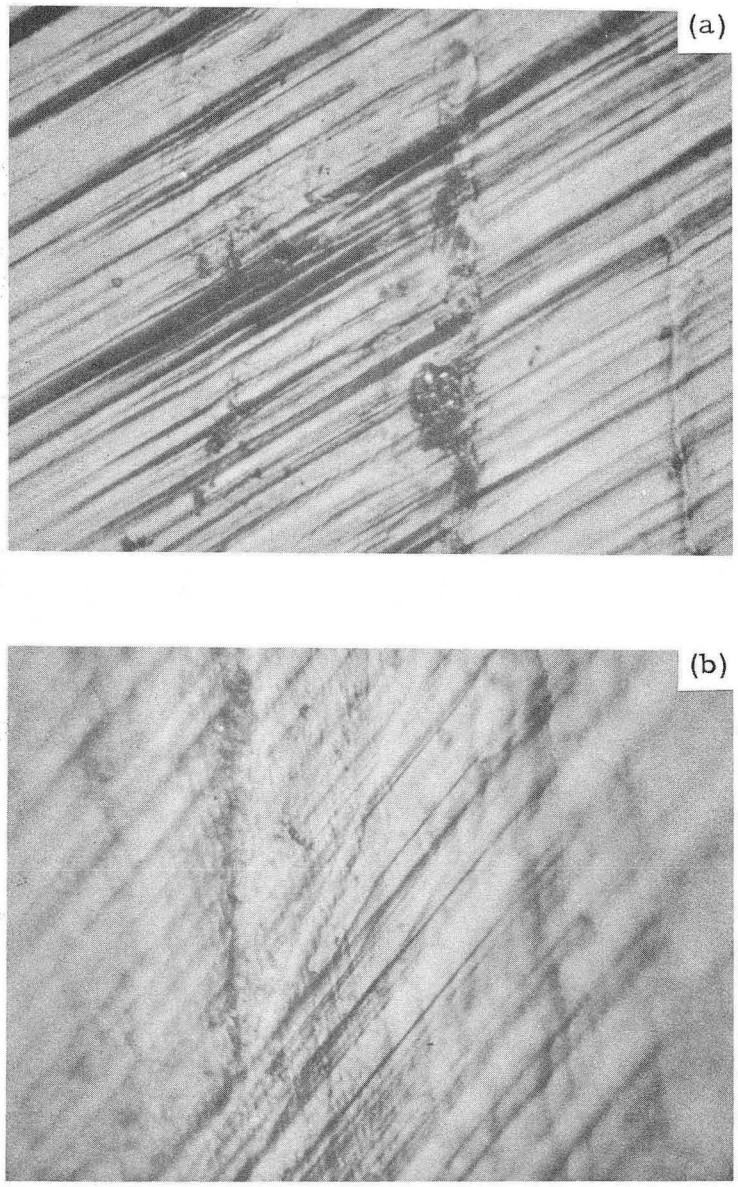

ZN-3431

Fig. 26. Cross-slip for tensile loads normal to the $(\bar{1}\bar{1}1)$ plane. 250X.
(a). $(\bar{1}10)$ face.
(b). (112) face.

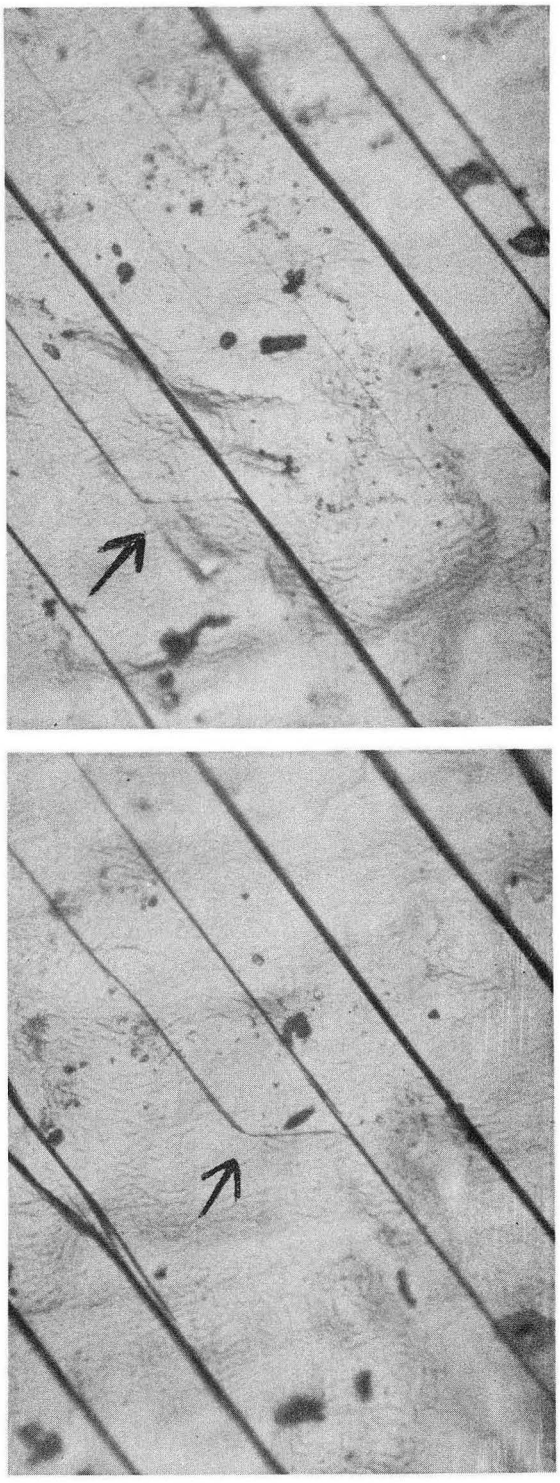

ZN-3432

Fig. 27. (112) surface of specimen pulled in tension normal to the $(\bar{1}\bar{1}1)$ plane at 170°C in air to 6% strain. 150X.

The cross-glide traces correspond very well to the $(0\bar{1}\bar{1})$ plane, as shown in Appendix D, which is perpendicular to the other $(0\bar{1}1)$ slip traces shown in Fig. 27.

Figure 28 shows the surfaces of a specimen pulled at 250°C with a tensile load normal to a $(\bar{1}\bar{1}1)$ plane. Part (a) of the figure, at a low magnification, shows the huge steps and cracks set in during deformation, while part (b) shows the appearance of wavy cracks on the surface. The cracks generally followed the {110} family of planes and appeared to produce much larger cracks and slip offsets than at the lower temperatures. The black areas surrounding the (112) plane surface of Fig. 28(b) are large cracks.

Figure 29 shows a trace on the surface of a specimen pulled in tension normal to the $(\bar{1}\bar{1}1)$ plane. This trace corresponded to within 5° of the (031) plane as calculated in Appendix E.

9. Discussion of the Mechanism of Cross-Slip

Figures 26 to 28 show that cross-slip occurred during deformation in cesium bromide. The mechanism by which cross-slip occurred is thought to be due to the glide of screw dislocations between perpendicular {110} planes. Figure 26(b) shows, for instance, that cross-slip may have occurred on a {100} plane. Screw dislocations might cross-slip on a {100} plane in a $\langle 100 \rangle$ direction because the Burger's vectors are properly oriented, but the calculated angle of intersection (see Appendix F) between the $(0\bar{1}0)$ and $(0\bar{1}1)$ planes on the $(\bar{1}\bar{1}\bar{2})$ plane deviates by about 10° from the experimental value as measured on Fig. 26(b). Slip on a {100} plane is also difficult because it necessitates an accumulation of charges of like sign at the surface, as schematically shown in Fig. 30(a). Therefore, slip in this case probably occurred by the cross-glide of screw dislocations between perpendicular {110} planes, in such a way as to form slip traces near a {100} plane. Figure 27 shows that cross-glide did occur between perpendicular {110} planes. Figure 30(b) shows how cross-slip on two perpendicular planes can form a slip trace that appears on a {100} plane.

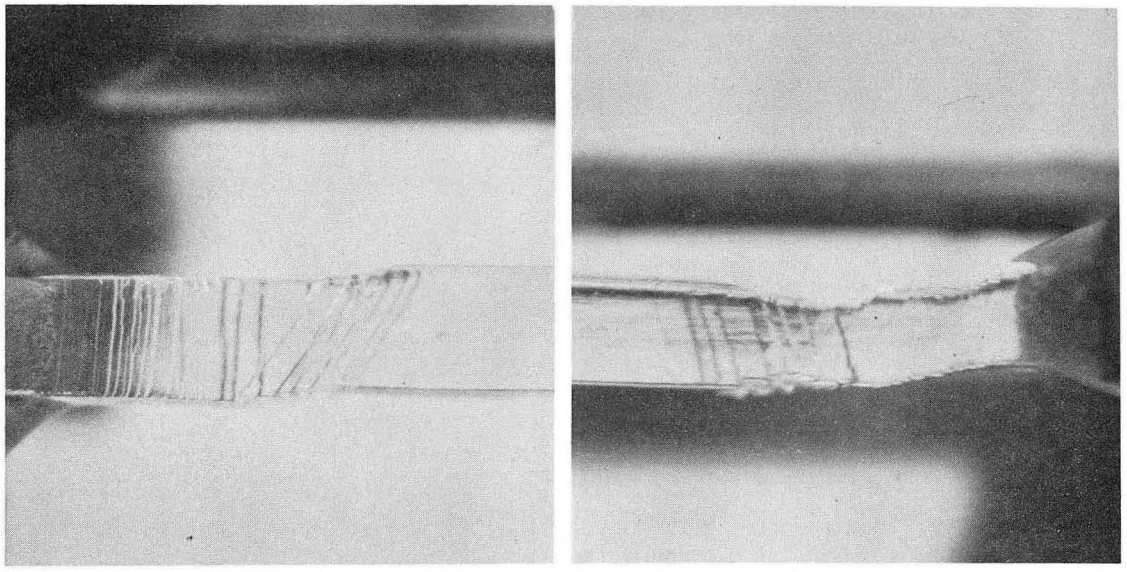

(112) face ($\bar{1}10$) face

(a). 6X.

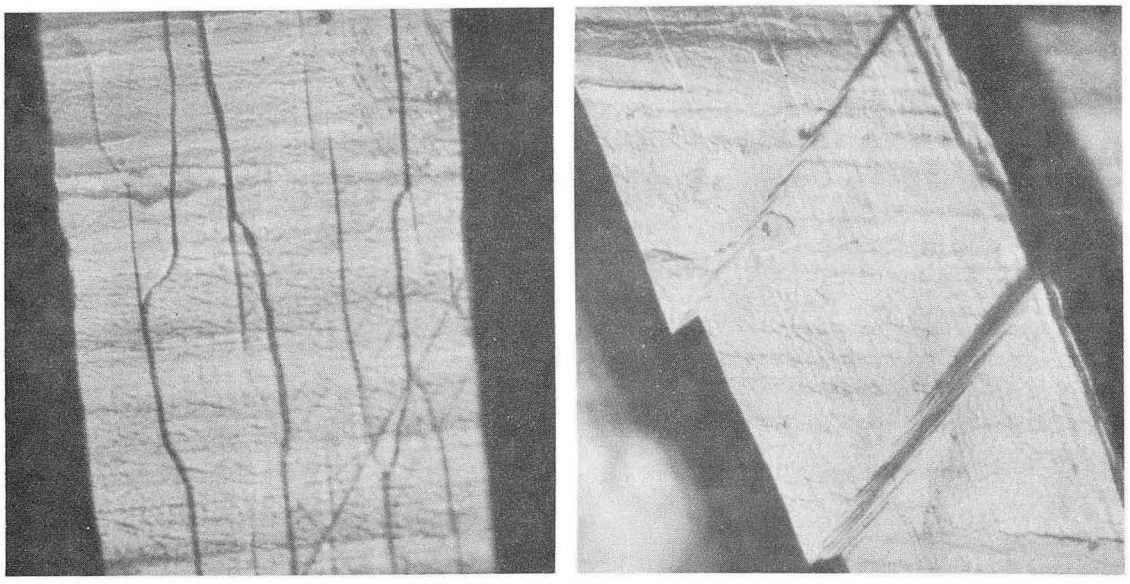

(112) face ($\bar{1}10$) face

(b). 150X.

Fig. 28. Slip traces of specimen pulled normal to ($\bar{1}\bar{1}1$) plane at 250° C in air.

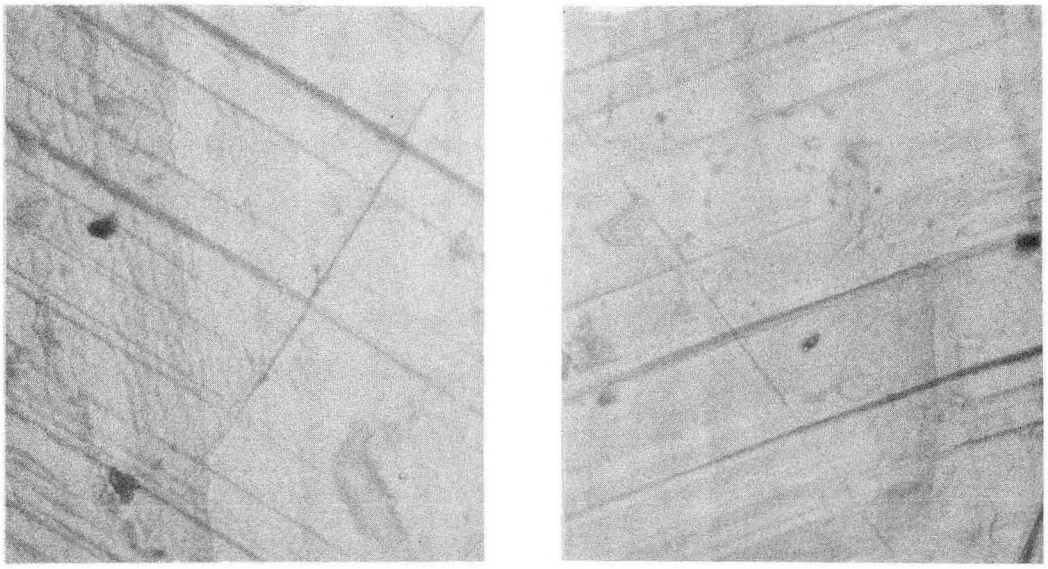

(112) face, 150X ($\bar{1}$10) face, 150X

(a). (031) slip trace with dominating ($\bar{1}$01) trace.

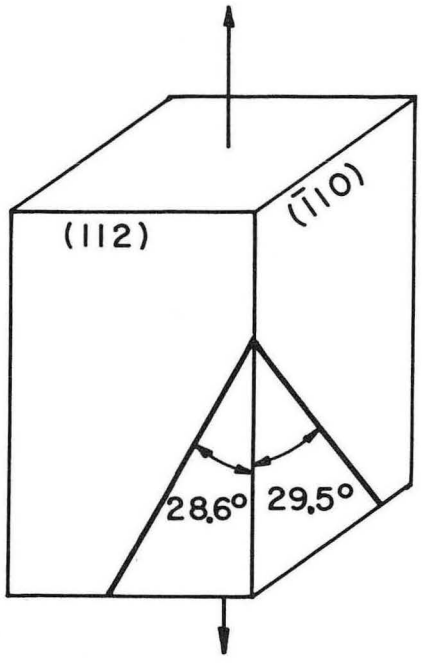

(b). Schematic mode of deformation for the (031) slip trace.

Fig. 29. Deformation in cesium bromide for the (031) trace for the 35° orientation.

ZN-3421

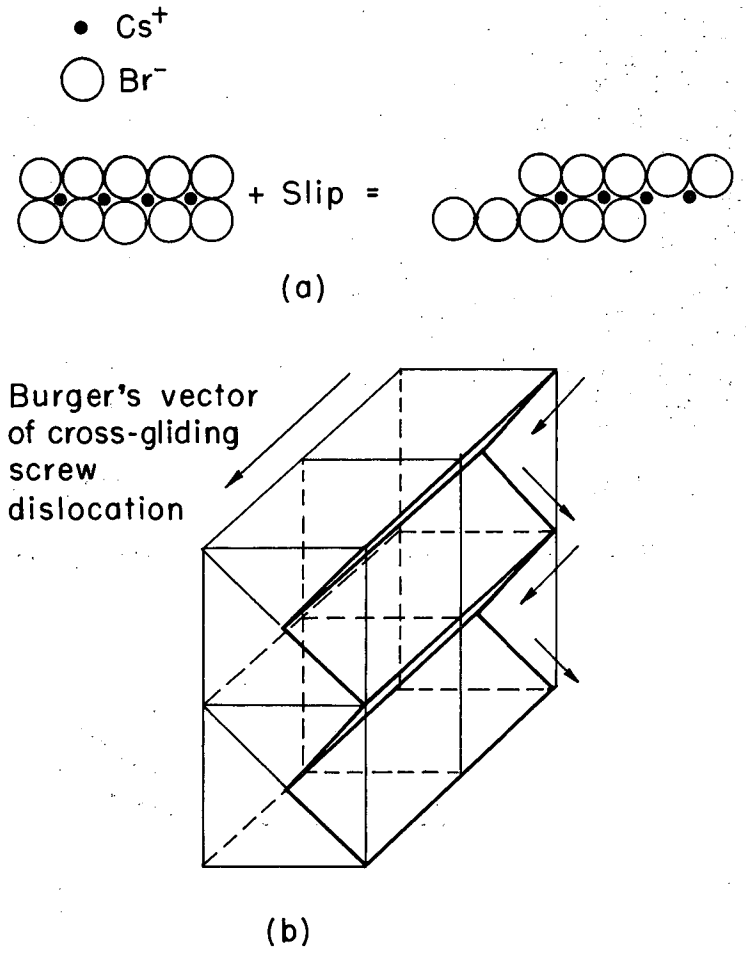

Fig. 30. Schematic diagrams concerning slip on the (010) plane.
(a). Slip on a {100} plane.
(b). Cross-slip on $(0\bar{1}1)$ and (011) planes to form jagged slip on the (010) plane.

The (031) trace seen in Fig. 29 may likewise be caused by screw dislocations oscillating between perpendicular {110} planes.

10. Mechanism of Fracture

Figure 31 shows photographs of fracture surfaces for specimens pulled normal to the (001) and (110) orientations. The angle of the fracture surfaces with the specimen edge coincided with {110} planes for a tensile load normal to the (001) and (110) planes. The fracture surface for a deflecting load on the (001) plane was again a {110} face, as shown in Fig. 32. Figure 32(c) shows cracks propagating along slip lines. Fracture was found on a {112} plane for a compression load normal to the (001) plane, as seen in Fig. 22, and was probably responsible for the largest drop in stress in the curve shown in Fig. 18. An examination of photographs of the {110} fractures indicated that the cracks progressed in $\langle 110 \rangle$ directions. Macroscopic observation of the fracture front on the (112) plane for the compression specimen indicated a $\langle 111 \rangle$ direction.

Figure 33 shows that cracks had formed along a $[1\bar{1}0]$ direction at dislocation-band intersections for tensile loads normal to the (110) plane. Figure 34 also shows photographs of cracks formed at dislocation intersections on the (001) plane of specimens pulled normal to the (110) plane. However, some of the surface lines did not coincide with the bands revealed by polarized light. This effect was due to the extensive amount of strain which had moved these surface lines. The cracks had opened along these intersections because of the large distortions and high stresses at the dislocation intersections.

11. Discussion of the Mechanism of Fracture

Fracture by tension in the single-crystal cesium bromide occurred through the progressive pulling apart of the ions and the consequential separation of ionic bonds. Fracture by compression, in contrast, occurred through the pushing of the ions together, which caused electrostatic repulsive forces and the consequential breakage of bonds. The mechanism

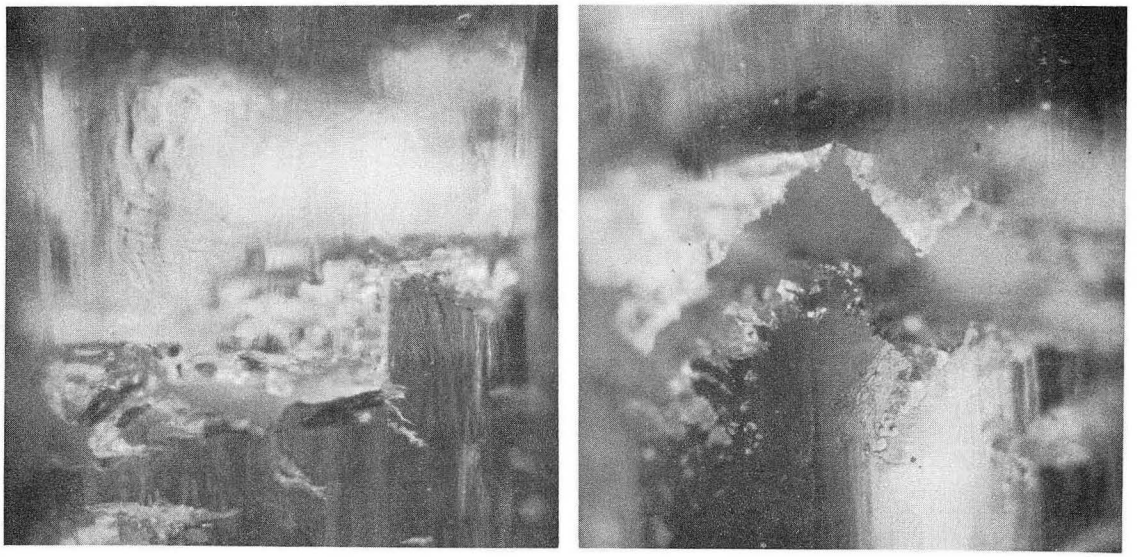

(a). Adjacent {100} surfaces for a tensile load normal to a {100} plane. Polarized light, 75X.

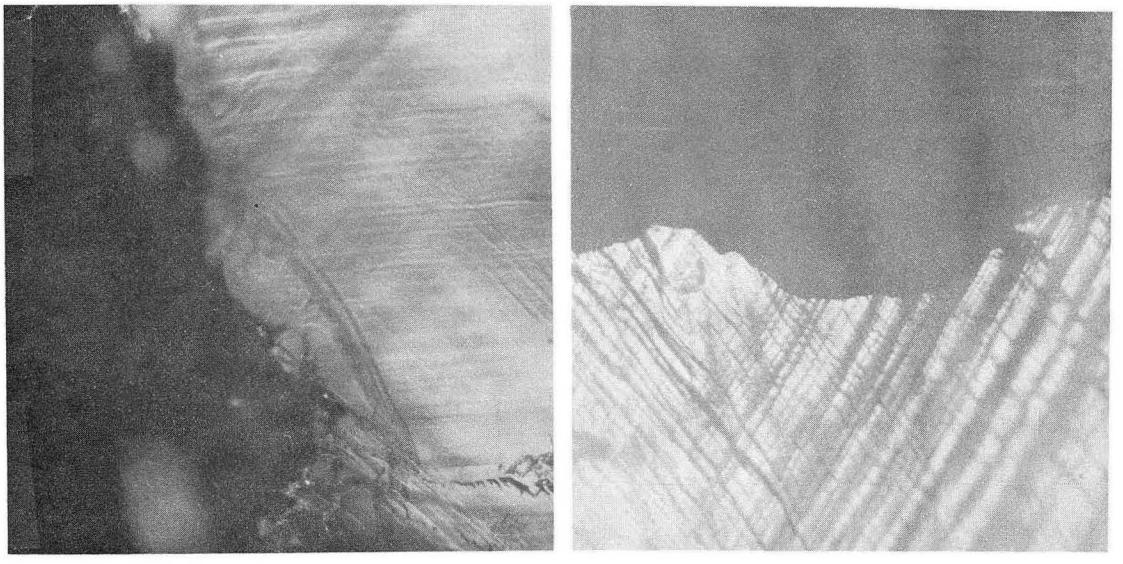

(001) plane, polarized light

(110) plane

(b). Adjacent surfaces for a tensile load normal to the (110) plane. 150X.

Fig. 31. Fracture surfaces of cesium bromide in tension.

(a). (010) side surface at tension edge.

(b). (010) side surface at compression edge.

(c). (001) tensile surface.

Fig. 32. Cracks in bend specimen oriented for load normal to the (001) plane. 150X.

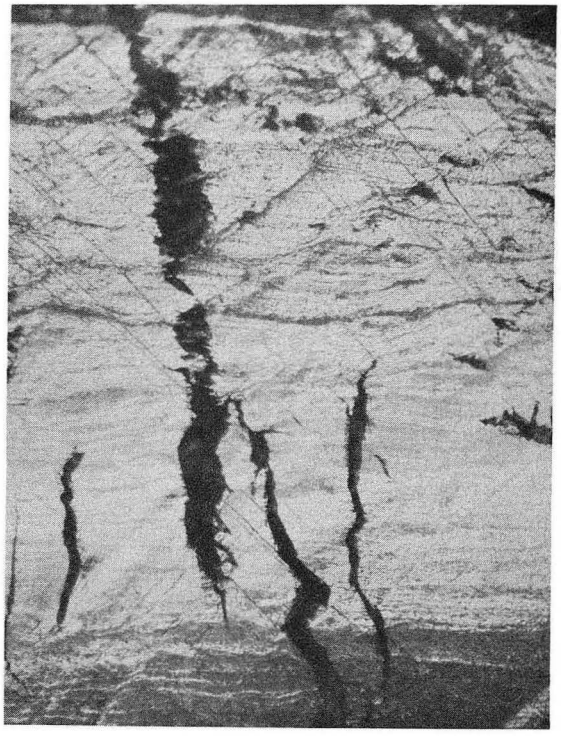

ZN-3433

Fig. 33. Crack formation along the [$1\bar{1}0$] direction on the (001) face for a tensile load normal to the (110) plane. 150X.

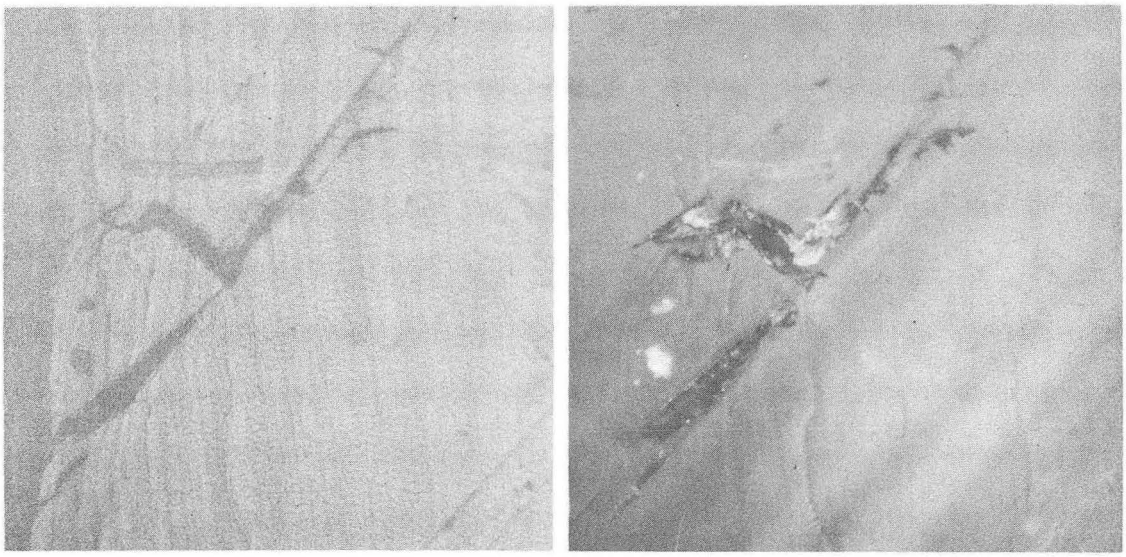

Regular light Polarized light

(a). First set of cracks.

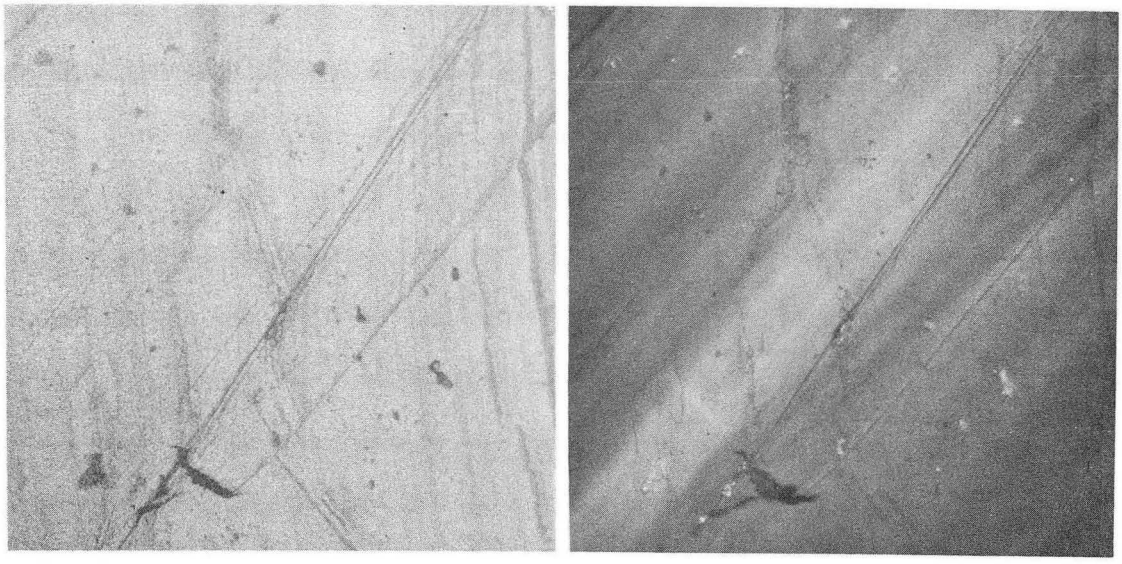

Regular light Polarized light

(b). Second set of cracks.

Fig. 34. Crack formation in cesium bromide single crystals pulled normal to the (110) plane, viewed on the (001) plane. 75X.

by which fracture occurred in the single-crystal cesium bromide could be explained on the basis of the amount of plastic strain in the material and the absence of cleavage planes. Since cesium bromide is soft and ductile, stress concentrations did not build up at the bottoms of cracks that formed during deformation, because the material flowed plastically to dissipate any buildup of stress at a crack tip. This analysis does not mean, however, that stress concentrations did not build up at dislocation intersections. Cracks in single-crystal cesium bromide, therefore, tended to grow in those directions on the fracture planes where the resolved shear stress was a maximum, unless there were stress concentrations in the material caused by dislocation intersections. The fracture planes in cesium bromide are $\{110\}$ and $\{112\}$ planes because an equal number of positive and negative ions are symmetrically distributed on these planes at separation to give an overall neutral charge. Because cleavage planes were not found in cesium bromide (down to $-196^{\circ}C$), there was no reason to suspect easier fracture on either one of these planes. Actually, the applied stresses necessary to cause fracture on both $\{110\}$ and $\{112\}$ planes for loads normal to a $\{100\}$ plane were about the same.

Cracks were often observed on the slip planes after deformation. These cracks had probably formed because of the decrease in cohesive energy between these planes, caused by the accumulation of dislocations on them.

Fracture occurred on the $\{110\}$ family of planes in tension rather than the $\{112\}$ family because of the following reaons. For the tensile loads normal to $\{100\}$ planes the resolved shear stress was a maximum for fracture on $\{110\}$ planes in $\langle 110 \rangle$ directions, as shown in Table I. Therefore, fracture should proceed in this manner, as found, in a soft material like cesium bromide. For the tensile loads normal to a (110) plane the maximum resolved shear was on the (112) plane in a $[\bar{1}\bar{1}1]$ direction, as shown in Table I, but fracture occurred on the (110) plane in an apparent $[1\bar{1}0]$ direction. This discrepancy was caused

Table I. Fracture modes for cesium bromide single crystals.

Orientation	Fracture system	Resolved shear ($\cos\theta\cos\lambda$)
$\sigma \perp \{100\}$	$\{110\}\langle 110\rangle$	$\cos 45^{\circ}\cos 45^{\circ}=0.5$
	$\{112\}\langle 111\rangle$	$\cos 35.3^{\circ}\cos 54.7^{\circ}=0.472$
	$\{110\}\langle 111\rangle$	$\cos 45^{\circ}\cos 54.7^{\circ}=0.408$
$\sigma_{\perp}$ (110)	$(112)\ [\bar{1}\bar{1}1]$	$\cos 54.7^{\circ}\cos 35.3^{\circ}=0.472$
	$(\bar{1}01)\ [111]$ or $(0\bar{1}1)\ [1\bar{1}1]$	$\cos 60^{\circ}\cos 35.3^{\circ}=0.408$
	$\{110\}\langle 100\rangle$	$\cos 60^{\circ}\cos 45^{\circ}=0.353$
	$\{110\}\langle 110\rangle$	$\cos 60^{\circ}\cos 60^{\circ}=0.25$

by the plastic deformation that occurred for tensile loads normal to the (110) plane, as compared to the lack of deformation for loads normal to a {100} plane. The fracture cracks for tensile loads normal to a (110) plane were nucleated at dislocation intersections, as shown in Figs. 33 and 34. These cracks propagated at an applied stress level of about one-tenth of that for those cracks propagated by a tensile load normal to a {100} plane, because of the stress concentrations which existed at the dislocation intersections. The stress concentrations were responsible for propagating the cracks on the plane of maximum shear, which in this case was the (110) plane.

Fracture occurred in compression on the {112} family of planes rather than the {110} planes for loads normal to a {100} plane, because the ions were pushed together rather than pulled apart. For compression loads normal to a {100} plane, cations were pushed together in a $\langle 100 \rangle$ direction (see Fig. 35), which created electrostatic repulsive forces. The ions consequently shifted and proceeded in a $\langle 111 \rangle$ direction because the electrostatic repulsive forces were least in this direction. (The ratio of distances of closest approach between cations would be $\sqrt{3}/\sqrt{2}$ for the $\langle 111 \rangle$ / $\langle 110 \rangle$ directions.) The material consequently fractured because the ionic bonds were not strong enough to withstand the electrostatic repulsive forces that were developed by the ions moving in a $\langle 111 \rangle$ direction. With the {100} direction, the {112} planes were favored over the {110} planes for fracture because the resolved shear was greater for {112} $\langle 111 \rangle$ fracture than {110} $\langle 111 \rangle$ fracture, as shown in Table I.

The fracture process for those specimens with tensile loads normal to the (110) and (001) planes was ductile in nature, as indicated by the slow drop in stress in the curves for the 90° and 0° orientations in Fig. 6. Figure 15 also shows that fracture was ductile for deflecting loads normal to the (001) plane (the other tests indicated in this figure were not carried to fracture).

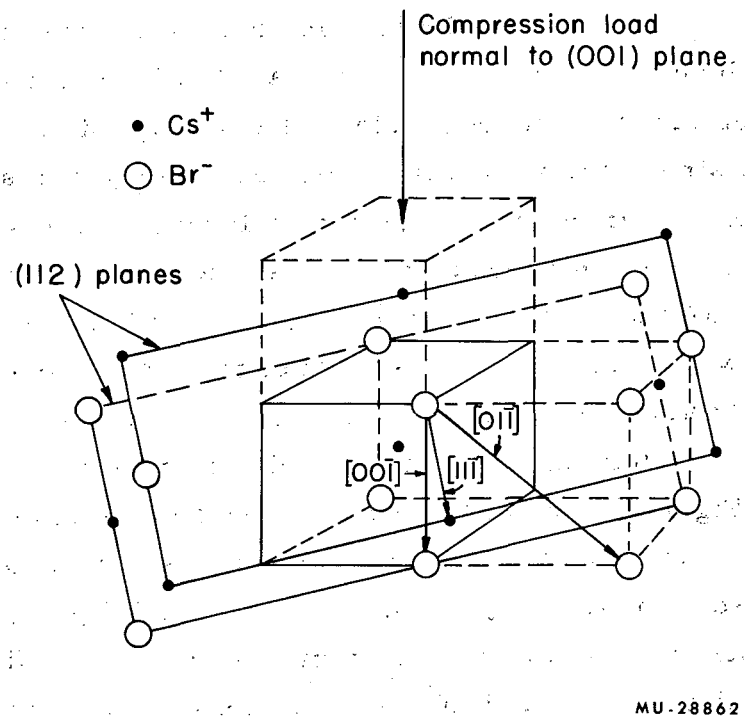

Fig. 35. Mechanism of fracture on the (112) plane in a $[11\bar{1}]$ direction for compression loads normal to the (001) plane.

B. Plastic-Deformation Behavior of Polycrystals

The following investigation is concerned with the effect of glide and grain size on the plastic-deformation behavior and of the lack of cleavage planes on the fracture behavior.

1. Mechanism of Plastic Deformation

Figure 36 shows the tensile characteristics of polycrystalline cesium bromide in air at 24°C for a < 325-mesh cold-pressed powder and a hot-pressed single crystal. The stress-strain curve of the hot-pressed single crystal showed more ductility (more strain before fracture) and curvature at a lower stress level than the < 325-mesh powdered compact. Photomicrographs of the surfaces of the tensile specimens in Figs. 37 and 38 show that the grain size of the hot-pressed single crystal was much greater than that of the < 325-mesh powdered compact. Figure 38 also shows slip traces in the hot-pressed single crystal and, therefore, deformation by glide within the grains.

Figure 39 shows the bending characteristics of polycrystalline cesium bromide in air at room temperature and at 300°C. The curves for the specimens bent at room temperature [Fig. 39(a)] show much higher stress levels than their counterpart [Fig. 39(b)] bent at 300°C. The specimens bent at 300°C also exhibited more strain than their counterpart bent at lower temperatures. The curves of Fig. 39 indicate that deformation was easier for the cold-pressed and hot-pressed single crystals than the < 325-mesh cold-pressed powder. A comparison of the photomicrographs of the surfaces of the bend specimens from Figs. 40 to 44 shows that the grains of the cold-pressed single crystal bent in the range of 50 to 100°C and the hot-pressed single crystal bent at 300°C were larger than the grains of the other three specimens. The grains of the cold-pressed single crystal bent at 300°C apparently were reduced by recrystallization that set in during the hour-long heating time to 300°C. The recrystallization was probably due to the stresses in the material caused by cold-pressing. The hot-pressed single crystal

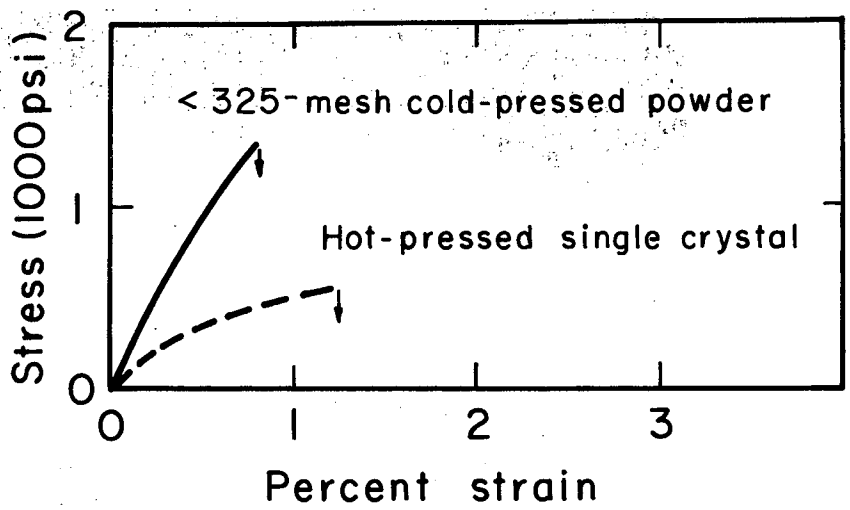

MU-28863

Fig. 36. Stress-strain curves of polycrystalline cesium bromide pulled in tension in air at 24°C on the Instron machine.

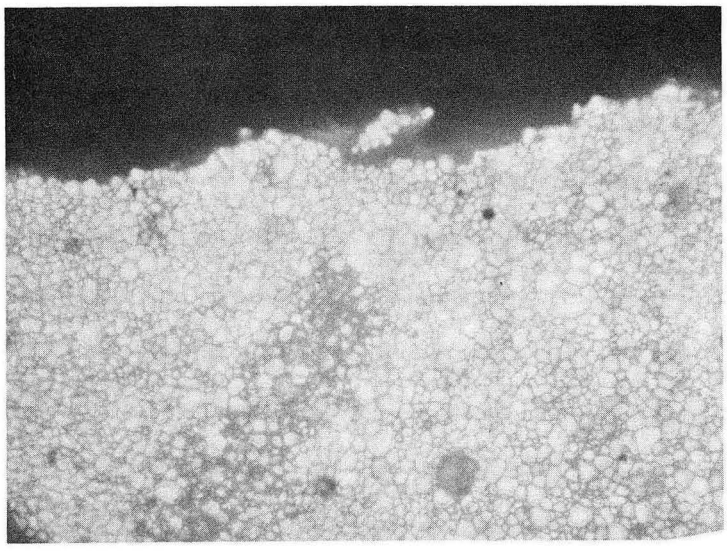

ZN-3434

Fig. 37. Intergranular fracture in < 325-mesh cold-pressed powder pulled in tension at 24°C. 150X.

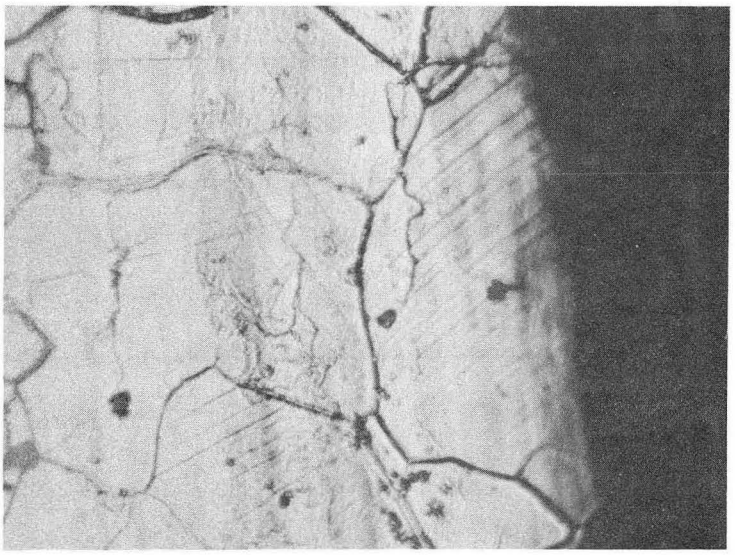

ZN-3435

Fig. 38. Slip traces in hot-pressed single crystal pulled in tension at 24°C. 150X.

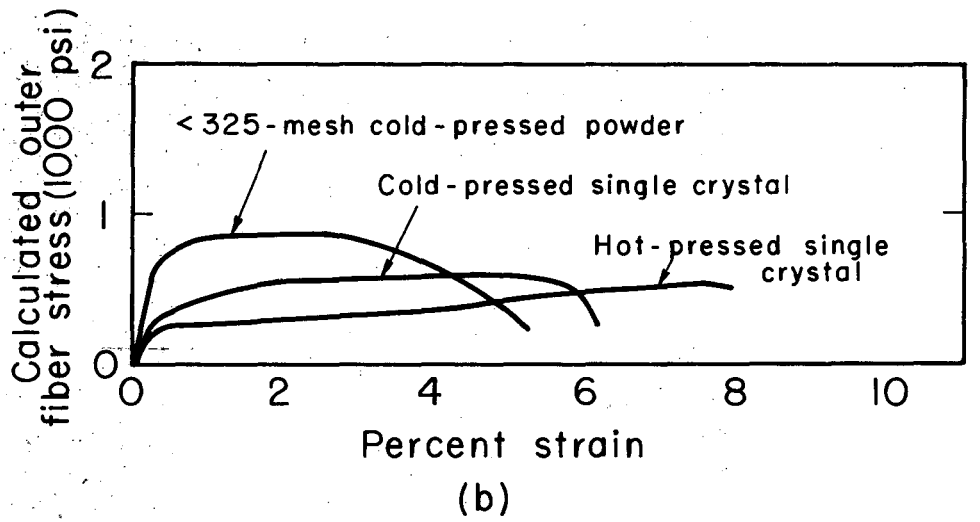

MU-28864

Fig. 39(a). Bending curves of polycrystalline cesium bromide in air at 24°C.

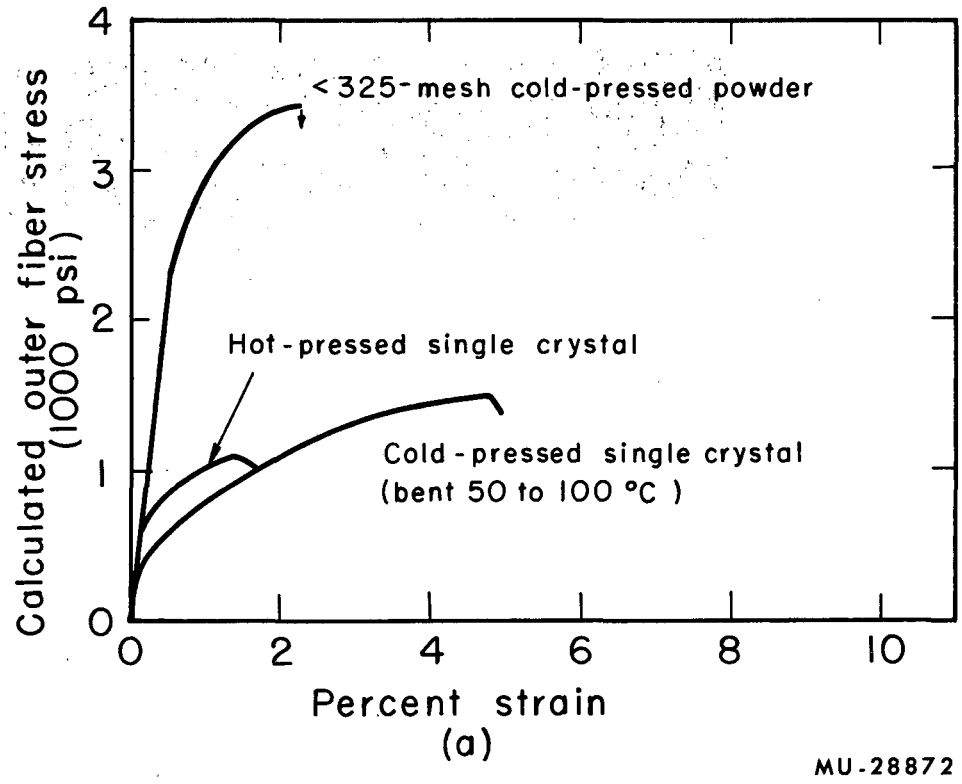

Fig. 39(b). Bending curves of polycrystalline cesium bromide in air at 300°C.

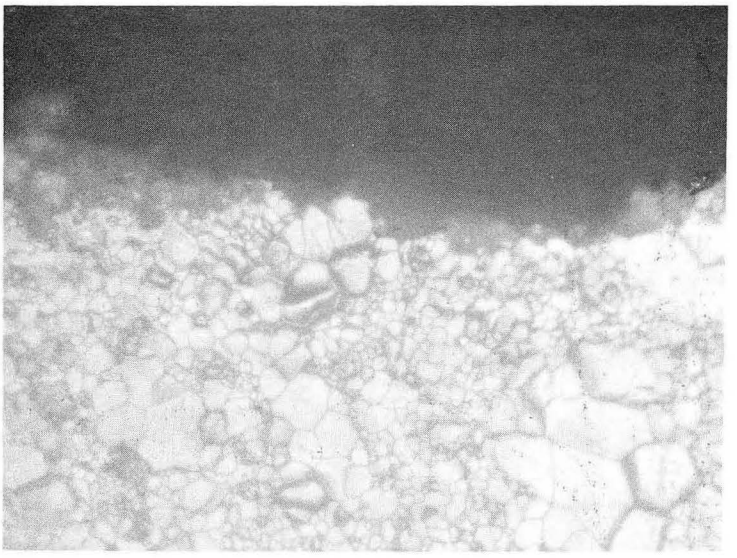

ZN-3436

Fig. 40. Intergranular fracture in < 325-mesh cold-pressed powder bent at 24°C. 150X.

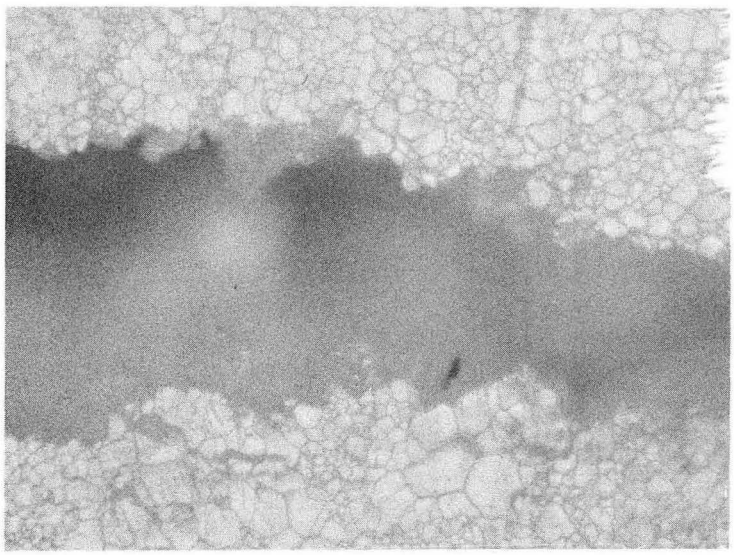

ZN-3437

Fig. 41. Intergranular fracture in < 325-mesh cold-pressed powder bent at 300°C. 150X.

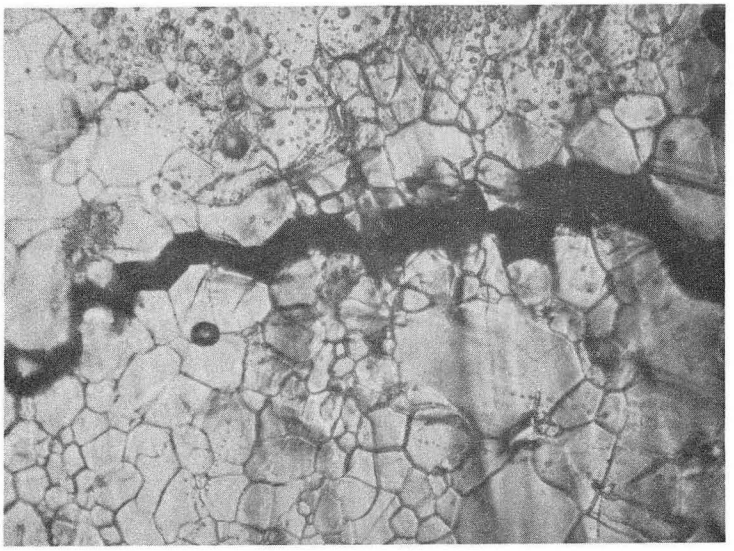

ZN-3438

Fig. 42. Intergranular fracture in cold-pressed single crystal bent at 50 to 100°C. 150X.

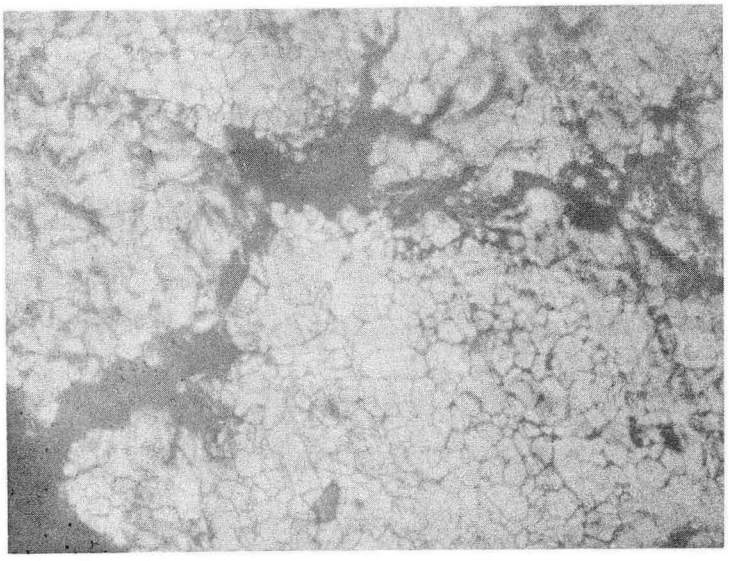

ZN-3439

Fig. 43. Intergranular fracture in cold-pressed single crystal bent at 300°C. 150X.

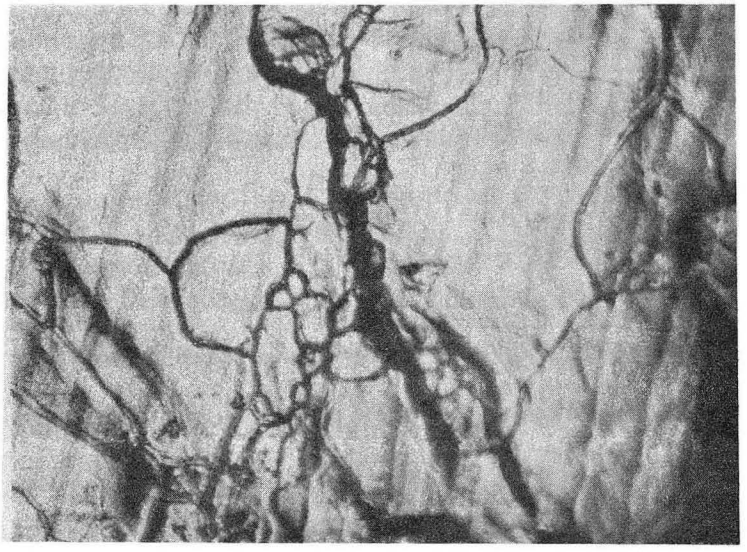

ZN-3440

Fig. 44. Intergranular fracture in hot-pressed single crystal bent at 300°C. 150X.

did not recrystallize during heating to 300°C because the stresses were annealed out by the hot-pressing treatment. Figures 45 and 46 show that slip occurred in the larger grained cold-pressed single crystal bent in the range of 50 to 100°C and in the hot-pressed single crystal bent at 24°C. Slip traces were also seen in the hot-pressed single crystal bent at 300°C.

A close examination of the slip traces of the hot-pressed single crystal in Figs. 38 and 46 showed that some slip traces had penetrated into neighboring grains, while others ended at the grain boundaries. A measurement of the deviation of the slip traces that penetrated through the grains indicated that the misorientation between the grains was relatively small. Figure 45 shows that the slip traces in the cold-pressed single crystal did not even reach the grain boundary, which indicated restraint of deformation at the grain boundaries and the relatively large misorientation between the grains. Apparently, the cold-pressed single crystal (Fig. 45) may have had larger-angle grain boundaries than the hot-pressed single crystal (Figs. 38 and 46).

2. Discussion of the Mechanism of Plastic Deformation

Figures 3 and 5 show that there are essentially no orientations for which a relatively high resolved shear stress exists on at least five slip systems for a given load. The Taylor theory,[21] however, requires the simultaneous operation of at least five systems of slip to prevent gaps or separations from forming between the grains within the aggregate. According to this theory, plastic deformation in cesium bromide should consequently be limited and, in fact, become less with smaller grain sizes, because of the restraint of deformation caused by the grain boundaries. The experimental results given below confirm the Taylor theory.

The results of the tension tests of polycrystalline cesium bromide pulled at 24°C show that deformation was small, and still less with smaller-grained material. Also, the photomicrographs show that glide occurred in the grains of the hot-pressed single-crystal sample in tension,

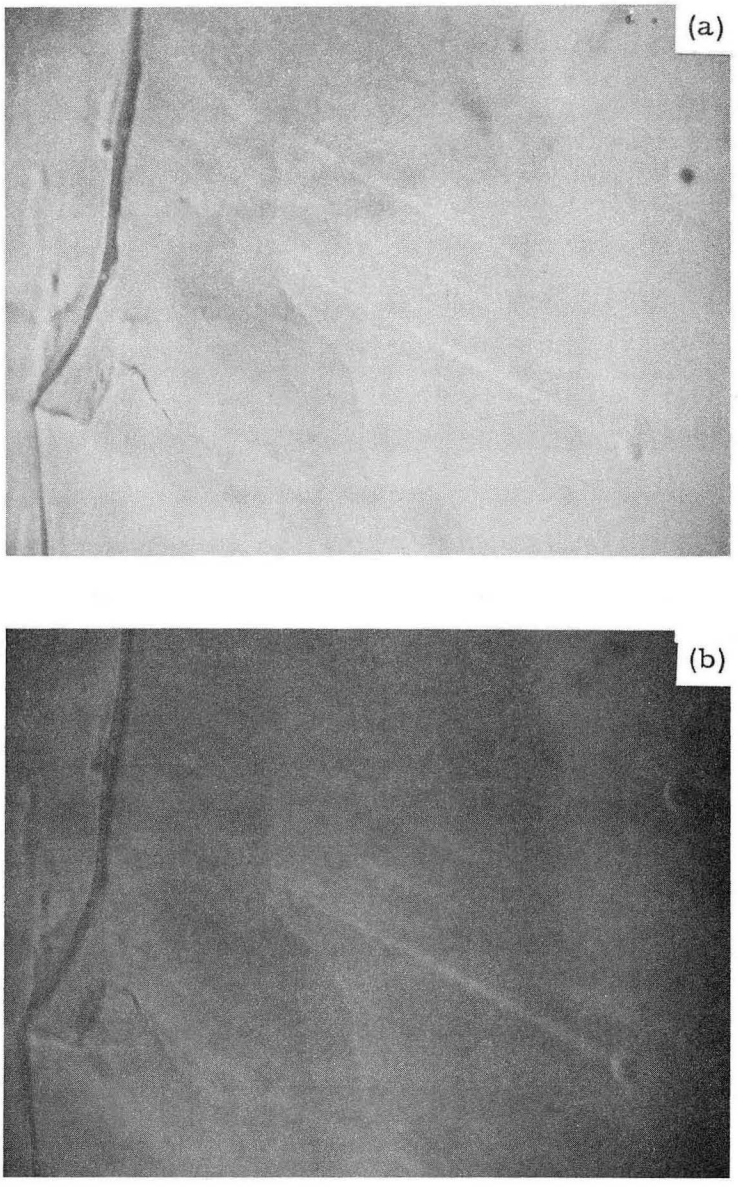

ZN-3441

Fig. 45. Slip traces in cold pressed single crystal bent at 50 to 100°C. 500X.
(a). Regular light.
(b). Polarized light.

ZN-3442

Fig. 46. Slip traces in hot-pressed single crystal bent at 24°C. 150X.

while slip bands were not detected in the < 325-mesh powdered compact which had the smaller size. This fact was reflected in a relatively higher tensile stress that was necessary to cause the same amount of strain in the < 325-mesh powdered compact.

Similarly, the bending data on polycrystalline cesium bromide show (a) that the larger-grained specimens had greater ductility than the smaller-grained < 325-mesh powdered compact at 300°C and (b) that glide occurred in the larger-grained specimens. Concrete evidence of slip in the fine-grained specimens could not be found. The stress values in bending of the < 325-mesh cold-pressed powder were also higher than those of the larger-grained pressed single crystals at room temperature and 300°C, which again indicates the difficulty for glide in the smaller-grained < 325-mesh cold-pressed powder.

At higher temperatures, the strain observed in the polycrystalline material probably resulted from grain-boundary shear and associated grain boundary separation, as well as deformation by glide. Cross-slip may have added to the plastic flow in the polycrystalline material, but it was apparently not significant enough at room temperature to provide enough additional slip systems to cause extensive plastic flow, particularly for the fine-grained specimens.

3. Mechanism of Fracture

Figures 37, 40 to 44, and 47 show that in every case fracture of polycrystalline cesium bromide was intergranular (between the grains) rather than transgranular (through the grains) or a combination of the two. This was a result of the lack of cleavage planes. The experimental data indicated that fracture of the single crystals for specimens with no plastic flow (loads normal to {100} planes) resulted at stress levels of about 5000 to 6000 psi. It was consequently not surprising that transgranular fracture did not appear, particularly because relatively few slip traces were seen on the surfaces of the polycrystalline specimens. The velocity of propagation of the intergranular fracture was also

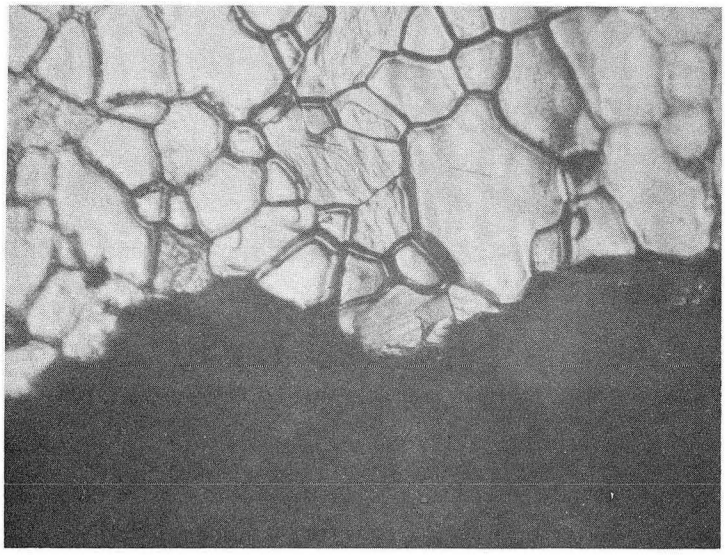

ZN-3443

Fig. 47. Intergranular fracture in hot-pressed single crystal pulled in tension at 24°C. 150X.

slow (ductile fracture) and became even slower at 300°C, as noted by the slow decrease in stress after fracture was first initiated [Fig. 39(b)].

4. Discussion of the Mechanism of Fracture

The photomicrographs show that the fracture process in polycrystalline cesium bromide was intergranular at 24 and 300°C, and that the ductility before fracture at 24°C was limited compared to the ductility of the single crystals in favorable orientations. In addition, Fig. 48 shows the grain-boundary surface of half of a bi-crystal that was separated during handling. These facts indicate weak attractive forces between the grains and reflect the lack of cleavage planes. Because it is known that CsCl, CsBr, and CsI are strongly polarizable,[24] the weak attractive forces at the grain boundaries were probably a result of van der Waals' bonding at the interfaces. The electrical forces of the ions at the surface of the grain are strongly decreased through polarication of the electron clouds. This induces a dipole and decreases the force field directed towards the surface of the adjacent crystal.

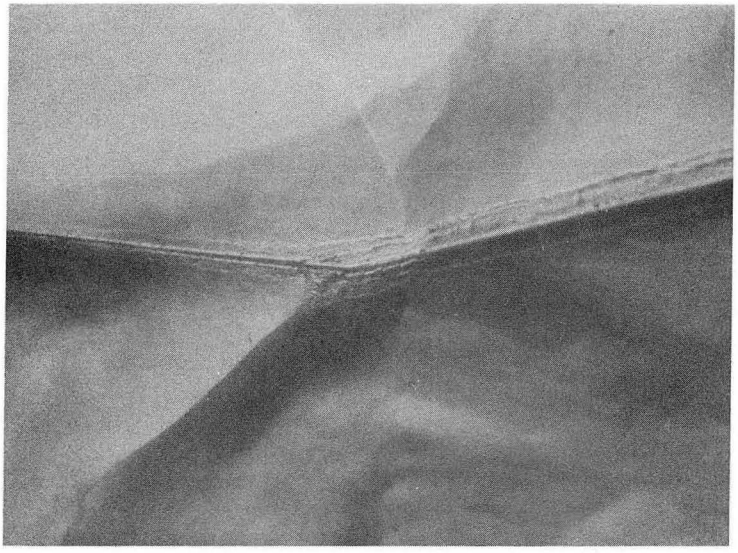

ZN-3444

Fig. 48. Grain boundary surface. 75X.

V. CONCLUSIONS

1. The $\{110\}\langle 100\rangle$ slip systems were the only glide systems activated during the tests, and these systems with the lack of cleavage made possible the considerable ductility of the single crystals stressed in favorable orientations. The resolved shear stress necessary to initiate flow on the glide systems was 126 psi.
2. Work-hardening in cesium bromide single crystals was caused by jogs that formed by the intersection of dislocations on slip planes at 60° to each other.
3. Kink bands suddenly formed in cesium bromide single crystals near an applied compression stress of 5000 psi normal to the $\{100\}$ family of planes; i.e., for orientations where no resolved shear stress existed on the $\{110\}\langle 100\rangle$ slip systems.
4. Ductile fracture, which preferentially occurred on $\{110\}$ planes in tension and bending, changed to $\{112\}$ planes in compression for loads normal to $\{100\}$ planes. This behavior was attributed to the lack of cleavage and the direction of load within the crystal. Cracks had not nucleated in the specimen for compression loads normal to a $\{110\}$ plane during deformation up to the strain investigated in the test.
5. Cracks often opened up along the $\{110\}\langle 100\rangle$ glide bands during deformation.
6. Cracks nucleated near slip bands and slip-band intersections in the material that plastically deformed by glide because of the stress concentrations at the dislocation intersections.
7. The amount of strain before fracture in polycrystalline cesium bromide was less for smaller grain sizes, indicating an insufficient number of slip systems available to overcome the grain-boundary restraint.
8. Deformation by glide contributed to the ductility of large-grained polycrystalline cesium bromide.
9. Polycrystalline cesium bromide fractured by an intergranular process up to 300°C because of the lack of cleavage planes and the weakness of the grain boundaries.

ACKNOWLEDGMENTS

The author wishes to thank Dr. Joseph A. Pask for his continuous support and guidance during the course of the experimental work. The suggestions of Dr. Gareth Thomas, Dr. Arthur F. Kip and S. Copley also valuably contributed to the worth of this investigation.

This work was done under the auspices of the U. S. Atomic Energy Commission.

APPENDICES

A. Calculation of the Resolved Shear Stress of the {110} ⟨100⟩ Slip Systems (see Fig. 49)

1. Calculation of the resolved shear stress for any orientation:

$$\cos\theta\cos\lambda = \frac{\mathbf{b}}{|\mathbf{b}|}(\cos a_1 \mathbf{i} + \cos a_2 \mathbf{j} + \cos a_3 \mathbf{k}) \times \frac{\mathbf{n}}{|\mathbf{n}|}(\cos a_1 \mathbf{i} + \cos a_2 \mathbf{j} + \cos a_3 \mathbf{k}),$$

where b is the Burger's vector and n is the normal of the plane.

a. $(1\,1\,0)[\,0\,0\,1\,]$

$$\frac{\mathbf{b}}{|\mathbf{b}|} = \mathbf{k}, \quad \frac{\mathbf{n}}{|\mathbf{n}|} = \frac{1}{\sqrt{2}}\mathbf{i} + \frac{1}{\sqrt{2}}\mathbf{j},$$

$$\cos\theta\cos\lambda = \cos a_3 \frac{(\cos a_1 + \cos a_2)}{\sqrt{2}}.$$

b. $(1\bar{1}0)[\,0\,0\,1\,]$

$$\frac{\mathbf{b}}{|\mathbf{b}|} = \mathbf{k}, \quad \frac{\mathbf{n}}{|\mathbf{n}|} = \frac{1}{\sqrt{2}}\mathbf{i} - \frac{1}{\sqrt{2}}\mathbf{j},$$

$$\cos\theta\cos\lambda = \cos a_3 \frac{(\cos a_1 - \cos a_2)}{\sqrt{2}}.$$

c. $(0\,1\,1)[\,1\,0\,0\,]$

$$\frac{\mathbf{b}}{|\mathbf{b}|} = \mathbf{i}, \quad \frac{\mathbf{n}}{|\mathbf{n}|} = \frac{1}{\sqrt{2}}\mathbf{j} + \frac{1}{\sqrt{2}}\mathbf{k},$$

$$\cos\theta\cos\lambda = \cos a_1 \frac{(\cos a_2 + \cos a_3)}{\sqrt{2}}$$

d. $(1\,0\,1)[\,0\,1\,0\,]$

$$\frac{\mathbf{b}}{|\mathbf{b}|} = \mathbf{j}, \quad \frac{\mathbf{n}}{|\mathbf{n}|} = \frac{1}{\sqrt{2}}\mathbf{i} + \frac{1}{\sqrt{2}}\mathbf{k},$$

$$\cos\theta\cos\lambda = \cos a_2 \frac{(\cos a_1 + \cos a_3)}{\sqrt{2}}.$$

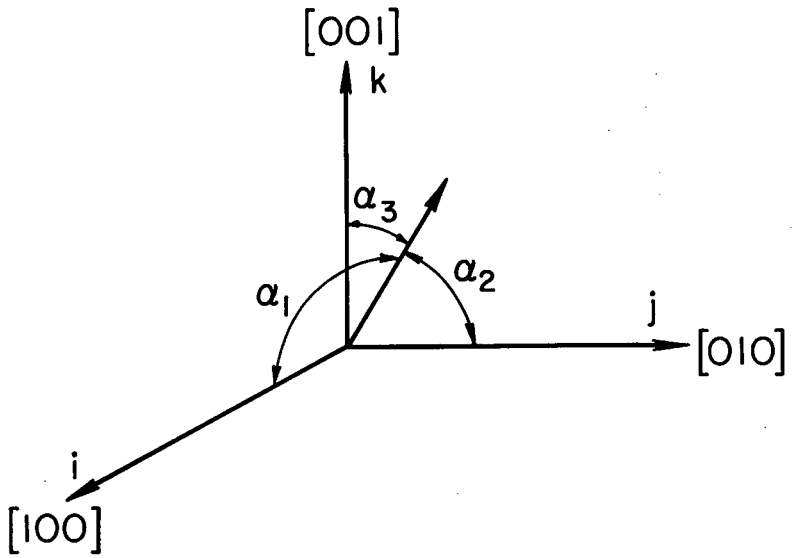

MU-28865

Fig. 49. Orientation of a_1, a_2, and a_3.

e. $(0\bar{1}1)[100]$

$$\frac{\overline{b}}{|\overline{b}|} = i, \quad \frac{\overline{n}}{|\overline{n}|} = -\frac{1}{\sqrt{2}}j + \frac{1}{\sqrt{2}}k ,$$

$$\cos\theta \cos\lambda = \cos a_1 \frac{(-\cos a_2 + \cos a_3)}{\sqrt{2}} .$$

f. $(\bar{1}01)[010]$

$$\frac{\overline{b}}{|\overline{b}|} = j , \quad \frac{\overline{n}}{|\overline{n}|} = -\frac{1}{\sqrt{2}}i + \frac{1}{\sqrt{2}}k ,$$

$$\cos\theta \cos\lambda = \cos a_2 \frac{(-\cos a_1 + \cos a_3)}{\sqrt{2}} .$$

2. Calculation of the resolved shear stress for $a_1 = a_2$, $a_3 = 90^\circ - a$ with:

$$\cos^2 a_1 + \cos^2 a_2 + \cos^2 a_3 = 1 ,$$

$$\cos^2 a_1 = \frac{\cos^2 a}{2} , \quad \cos a = \sin a_3 .$$

a. $(110)[001]$

$$\cos\theta \cos \quad = \frac{2}{\sqrt{2}} \cos a_3 \cos a_1 = \cos a \sin a .$$

b. $(1\bar{1}0)[001]$

$$\cos\theta \cos\lambda = 0 .$$

c. $(011)[100]$ or $(101)[010]$

$$\cos\theta \cos\lambda = \frac{\cos^2 a_1}{\sqrt{2}} \frac{\cos a_1 \cos a_3}{\sqrt{2}} = \frac{\cos^2 a}{2\sqrt{2}} (1 \pm \sqrt{2} \tan a) .$$

d. $(0\bar{1}1)[100]$ or $(\bar{1}01)[010]$

$$\cos\theta \cos\lambda = -\frac{\cos^2 a_1}{\sqrt{2}} + \frac{\cos a_1 \cos a_3}{\sqrt{2}} = -\frac{\cos^2 a}{2\sqrt{2}} (1 \mp \sqrt{2} \tan a).$$

B. Calculation of the Angles of the {110} Slip Traces Intersecting the Surfaces for Various Angles of Alpha

1. Alpha = 0°, slip traces are $(\bar{1}01)[010]$, $(011)[100]$

   a. Angle on (001) surface

   $$\theta = \frac{90}{2} = 45^{\circ}.$$

   b. Angle on $(\bar{1}10)$ surface

   $$\tan\theta = \frac{1}{\sqrt{2}}$$

   $$\theta = 35.3^{\circ}.$$

2. Alpha = 15°, slip trace is $(\bar{1}01)[010]$

   a. Angle on the alpha = 15° surface

   $$CD = \sqrt{2}$$

   $$DB = \frac{\sqrt{2}}{\cos 15^{\circ}}$$

   $$CB = (4 + 2\tan^2 15^{\circ})^{1/2} = 2.035$$

   $$(CD)^2 = (DB)^2 + (CB)^2 - 2(DB)(CB)\cos\theta$$

   $$\cos\theta = 0.743$$

   $$\theta = 42^{\circ}.$$

   b. Angle on $(\bar{1}10)$ surface

   $$\theta = 35.3^{\circ} + 15^{\circ} = 50.3^{\circ}.$$

3. Alpha = 29°, slip trace is $(\bar{1}01)[010]$

   a. Angle on the alpha = 29° surface

   $$CD = \sqrt{2}$$

   $$DB = \frac{\sqrt{2}}{\cos 29^{\circ}}$$

   $$CB = (4 + 2\tan^2 29^{\circ})^{1/2} = 2.15$$

   $$(CD)^2 = (DB)^2 + (CB)^2 - 2(DB)(CB)\cos\theta$$

   $$\cos\theta = 0.753$$

   $$\theta = 41^{\circ}.$$

b. Angle on $(\bar{1}10)$ surface

$\theta = 35.3^{\circ} + 29^{\circ} = 64.3^{\circ}$.

4. Alpha = 35.3°, slip traces are $(0\bar{1}1)[100]$, $(\bar{1}01)[010]$, $(110)[001]$

a. Angles on (112) surface

(1). θ of $(110) = 90^{\circ}$

(2). θ of $(0\bar{1}1)$, $(\bar{1}01)$

$$\tan\theta \frac{2\sqrt{2}}{\sqrt{3}}$$

$\theta = 58.5^{\circ}$.

b. Angles on $(\bar{1}10)$ surface

(1). θ of $(110) = 90^{\circ} - 35.3^{\circ} = 54.7^{\circ}$

(2). θ of $(0\bar{1}1)$, $(\bar{1}01) = 35.3^{\circ} + 35.3^{\circ} = 70.6^{\circ}$.

C. Angle of Intersection of the $(0\bar{1}\bar{1})$ and $(\bar{1}0\bar{1})$ Planes on the $(\bar{1}\bar{1}1)$ Surface (see Fig. 50)

EF: $(0\bar{1}\bar{1})$ trace

AC: $(\bar{1}0\bar{1})$ trace

$$AB = \sqrt{\frac{3}{2}}$$

$$CB = \sqrt{\frac{2}{2}}$$

$$AC = \sqrt{2}$$

$$\cos\angle CAB = \frac{3}{\sqrt{2}\sqrt{2}} = \sqrt{\frac{3}{2}}$$

$$\angle CAB = 30^{\circ}$$

$$AF = \sqrt{\frac{2}{2}}$$

$$EF = \sqrt{\frac{3}{2}}$$

$$(AF)^2 = (AE)^2 + (EF)^2 - 2(AE)(EF)\cos\angle FEA$$

$$\cos\angle FEA = \frac{3}{2\sqrt{3}}$$

$$\angle FEA = 30^{\circ}.$$

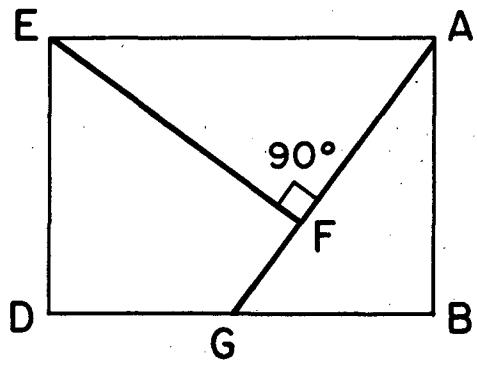

MU-28866

Fig. 50. Angle of intersection of the $(0\bar{1}\bar{1})$ and $(\bar{1}0\bar{1})$ planes on the $(\bar{1}\bar{1}1)$ surface.

D. Angle of Intersection of $(0\bar{1}\bar{1})$ and $(01\bar{1})$ Planes on the $(\bar{1}\bar{1}2)$ Surface (see Fig. 51)

$$\theta = 90^\circ - \angle AGB = \angle ABC$$

$$\tan\angle AGB = \frac{\sqrt{3}}{2\sqrt{2}}$$

$$\angle AGB = 31.5^\circ$$

$$\theta = 90^\circ - 31.5^\circ = 58.5^\circ .$$

E. Angle of Intersection of the (031) Plane with the Specimen Surface for the 35.3° Orientation (see Fig. 52)

1. $\theta_{(112)} = \angle DAB$

$$\tan\theta_{(112)} = \frac{2\sqrt{2}}{3\sqrt{3}}$$

$$\theta_{(112)} = 28.6^\circ .$$

2. $\theta_{(\bar{1}10)} = \angle DAC$

$$\tan\angle CAO = \sqrt{\frac{2}{3}}$$

$$\angle CAO = 25.2^\circ$$

$$\theta_{(\bar{1}10)} = 54.7 - \angle CAO = 29.5^\circ .$$

F. Angle of Intersection of $(0\bar{1}0)$ and $(0\bar{1}1)$ Planes on the $(\bar{1}\bar{1}2)$ Surface (see Fig. 53)

$$\theta = \angle CBA - \angle CBG = \angle ABE$$

$$\tan\angle CBG = \frac{\sqrt{3}}{2\sqrt{2}}$$

$$\angle CBG = 31.5^\circ$$

$$\tan\angle CBA = \sqrt{\frac{3}{2}}$$

$$\angle CBA = 50.8^\circ$$

$$\theta = 50.8^\circ - 31.5^\circ = 19.3^\circ .$$

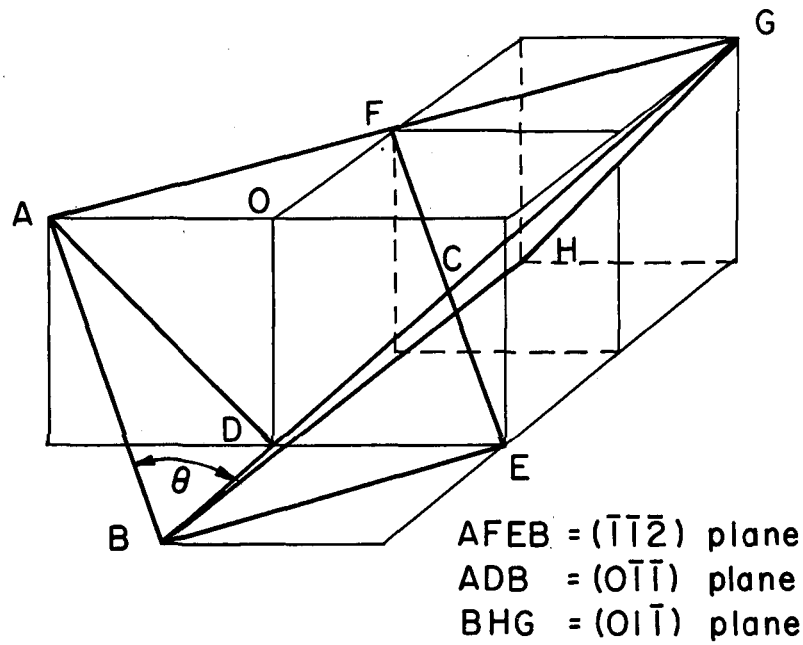

MU-28867

Fig. 51. Angle of intersection of the $(0\bar{1}\bar{1})$ and $(01\bar{1})$ planes on the $(\bar{1}\bar{1}\bar{2})$ surface.

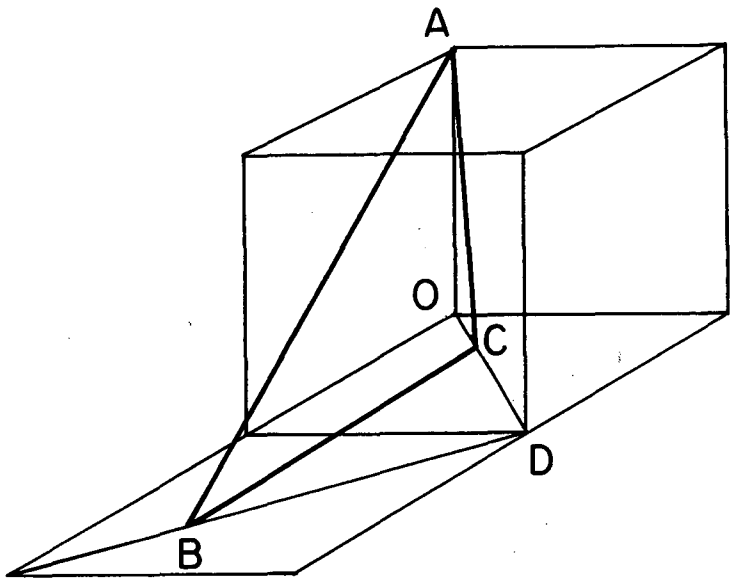

MU-28868

Fig. 52. Intersection of the (031) slip trace with the specimen surface for the 35.3° orientation.

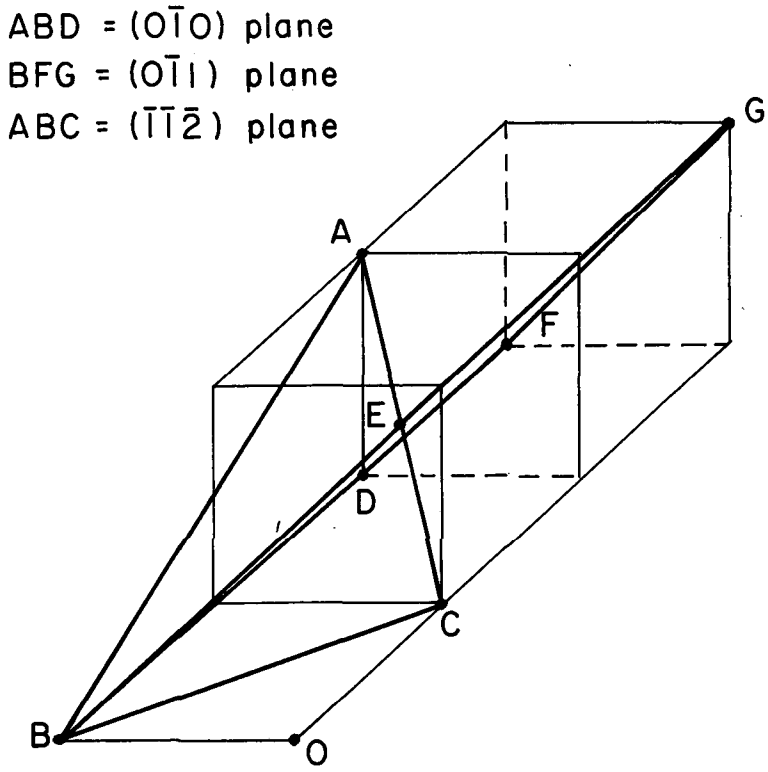

Fig. 53. Angle of intersection of the (0$\bar{1}$0) and (0$\bar{1}$1) planes on ($\bar{1}\bar{1}$2) surface.

REFERENCES

1. W. D. Scott, Deformation and Fracture of Polycrystalline LiF (Ph. D. Thesis), University of California, Berkeley, Sept. 1961 (unpublished).
2. S. Feuerstein, The Effect of Grain Boundaries on the Mechanical Properties of Ionic Crystals, University of California, Berkeley, Institute of Engineering Research Report Series 150, Issue No. 5, Jan. 1962 (unpublished).
3. A. R. C. Westwood, On the Fracture Behavior of MgO Bi-crystals, Phil. Mag., 6, 195 (1961).
4. R. J. Stokes and C. H. Li, The Tensile Strength of MgO, Office of Naval Research Project Nonr-2456(00) NR-032-451, 16th Technical Reprint, Honeywell Research Center, Hopkins, Minnesota, June 1962 (unpublished).
5. A. Smakula and M. W. Klein, The Plastic Deformation and Crystal Orientation of Thallium Halides, J. Opt. Soc. Am. 39, 445-53 (1949).
6. A. A. Urusovskaya, Figures of Plastic Deformation Observed on Crystals of Thallium Bromide-Thallium Iodide, Cesium Iodide, and Cesium Bromide, Tr. Inst. Kristallogr., Akad. Nauk SSSR 12, 172-9 (1956)
7. W. A. Rachinger and A. H. Cottrell, Slip in Crystals of Cesium Chloride Type, Acta Met. 4, 109-13 (1956).
8. M. V. Klassen-Neklyudova, A. A. Urusovskaya, "Open-work Figures from Impact and Pressure in Cubic Crystals", Tr. Inst. Kristallogr. Akad. Nauk SSSR 11, 146-51 (1955).
9. A. H. Cottrell, Dislocations and Plastic Flow in Crystals (Oxford University Press, Amen House, London, 1956).
10. A. B. Zemtsov, M. V. Klassen-Neklyudova, and A. A. Urusovskaya, The Complicated Phenomenon of Plastic Deformation of Monocrystals, Doklady Akad Nauk SSSR 91, 813-6 (1953).

11. E. Orowan, A New Type of Plastic Deformation in Metals, Nature 149, 643-4 (1942).

12. E. V. Kolontsova, I. V. Telegina, and G. M. Plavnik, The Structure of Band Faults (Kink Bands) in Certain Ionic Crystals, Kristallografiya 1, 419-24 (1956).

13. E. V. Kolontsova and I. V. Telegina, A Possible Mechanism of Twinning in Cesium Iodide and Cesium Bromide Crystals, Soviet Phys. -Cryst. 3, 337-40 (1958).

14. E. V. Kolontsova and I. V. Telegina, Mechanism for the Formation of Fault Zones, Doklady Akad. Nauk SSSR 116, 605-8 (1957).

15. M. V. Klassen-Neklyudova and A. A. Urusovskaya, Plastic Deformation of Crystals Caused by Rotation of Lattice Without Formation of Glide Lines, Soviet Phys. -Cryst. 2, 128-33 (1957).

16. M. V. Klassen-Neklyudova and A. A. Urusovskaya, Effect of Heterogeneous Stress on the Mechanism of Plastic Deformation of Thallium and Cesium Halides, Kristallografiya 1, 410-18 (1956).

17. R. J. Stokes, T. L. Johnston, and C. H. Li, Kinking and the Fracture of Ionic Solids, Office of Naval Research Project Nonr-2456(00)NR-032-451, 12th Technical Report, Honeywell Research Center, Hopkins, Minnesota, June 1961 (unpublished).

18. V. R. Regel, The Problem of Dependence of the Range of Plasticity of Monocrystals on the Temperature and Velocity of Deformation, Akad Nauk SSSR, Inst. Met. im. A. A. Baikova, 2, 275-80 (1957).

19. V. R. Regel and G. E. Tomilovskii, The Dependence of the Creep Strength of the Single Crystals of TlBr-TlI Upon the Deformation Rate and the Temperature, Tr. Inst. Kristallogr., Akad. Nauk SSSR 12, 158-164 (1956).

20. E. Schmid and W. Boas, Plasticity of Crystals, with Special Reference to Metals (F. A. Hughes, London, 1950).

21. G. I. Taylor, Analysis of Plastic Strain in a Cubic Crystal, J. Inst. Metals 62, 307 (1938).

22. R. J. Stokes and C. H. Li, Dislocations and the Strength of Polycrystalline Ceramics, Office of Naval Research Project Nonr-2456(00)NR-032-451, 15th Technical Report, Honeywell Research Center, Hopkins, Minnesota, 1962 (unpublished).

23. M. A. Adams and G. T. Murray, Grain Boundary Sliding in Non-metallic Bi-crystals, Materials Research Corporation, Yonkers N. Y., Final Report on Contract AF(30-1)-2178, 1960 (unpublished).

24. T. Neugebauer, Transition from Homopolar to Ionic Bond, Naturwissenschaften 40, 459-60 (1953).